Informational active matter

Bryan VanSaders[1] and Vincenzo Vitelli[1, 2, 3, *]

[1] *James Franck Institute, The University of Chicago, Chicago, Illinois 60637, USA*
[2] *Department of Physics, The University of Chicago, Chicago, Illinois 60637, USA*
[3] *Kadanoff Center for Theoretical Physics, The University of Chicago, Chicago, Illinois 60637, USA*

(Dated: February 16, 2023)

Many biomolecular systems can be viewed as ratchets that rectify environmental noise through measurements and information processing. As miniaturized robots cross the scale of unicellular organisms, on-board sensing and feedback open new possibilities for propulsion strategies that exploit fluctuations rather than fight them. Here, we study extended media in which many constituents display a feedback control loop between measurement of their microstates and the capability to bias their noise-induced transitions. We dub such many body systems informational active matter and show how information theoretic arguments and kinetic theory derivations yield their macroscopic properties starting from microscopic agent strategies. These include the ability to self-propel without applying work and to print patterns whose resolution improves as noise increases. We support our analytical results with extensive simulations of a fluid of 'thinker' type particles that can selectively change their diameters to bias scattering transitions. This minimal model can be regarded as a non-equilibrium analogue of entropic elasticity that exemplifies the key property of this class of systems: self-propulsive forces grow ever stronger as environmental noise increases thanks to measurements and control actions undertaken by the microscopic constituents. We envision applications of our ideas ranging from noise induced patterning performed by collections of microrobots to reinforcement learning aided identification of migration strategies for collections of organisms that exploit turbulent flows or fluctuating chemotactic fields.

arXiv:2302.07402v1 [cond-mat.soft] 14 Feb 2023

The processes of life are informational in nature [1]. In its simplest incarnation a biological organism is endowed with two key capabilities: a *receptive* one that senses the environment the organism interacts with, and an *active* one used to affect control over, or motion through, that environment. Crucially, feedback between receptivity and action is needed, which entails information processing capabilities. At submicron scales where thermal fluctuations dominate, biomolecular machines central to transmembrane transport [2], chemical sensing [3–5], and transcription [6, 7] resort to memory-like structures to rectify noise into motion. Even at macro scales, organisms make decisions to harness fluctuating food sources [8] or migration conditions [9, 10]. Moreover, as microrobots shrink, the need grows for exploiting (rather than fighting) environmental noise through on-board sensing and feedback control [11–14].

An idealized example of such noise rectification is the 'information ratchet' shown in Fig. 1a. Subject to the outcome of measurements of the random forces on the ratchet, a frictionless pawl is selectively inserted to block counterclockwise transitions. Such a feedback protocol can favor clockwise motion without the need of performing any work on the ratchet (aside from memory erasure, as in the Maxwell demon paradox [15–21]), because thermal fluctuations are supplying the forces. Complex biomolecular machines, such as the protein RNA polymerase [22] shown in Fig. 1b can be modelled as information ratchets [23–28]. As it moves along a DNA template, the polymerase builds an RNA strand from the template by biasing the random addition of bases, ultimately growing the strand only in the direction of the correct sequence (i.e. down the template). This way of navigating a noisy environment contrasts with the method typically used by synthetic swimmers or active colloids powered by catalytic reactions, that directly push against environmental noise with rocket-like propulsion [29–41]. Crucially, such 'worker'-type particles must dissipate energy fighting noise, while informational ratcheting agents turn noise into a useful motive force whose amplitude grows as environmental fluctuations increase. Information ratchets are therefore reminiscent of entropic springs that get stiffer as thermal fluctuations increase. However, entropic elasticity is an equilibrium phenomenon: stiffness increases with the number of available microstates, as the temperature is raised [42]. What sets information ratchets apart from entropic springs is their ability to break detailed balance, as they bias transitions among microstates.

Information ratchets have long been studied mostly as individual objects, notably in the context of molecular motors [26, 43–48]. Here, we focus on extended media where many constituent particles interact with each other using their information ratcheting capabilities and control actions [49]. More explicitly, these 'thinker-type' agents can execute the following actions:

i. measure their respective microstates,
ii. bias noise-driven transitions between microstates,
iii. establish a feedback loop between (i) and (ii),
iv. operate with finite resources, e.g. the mechanical work W agents can exert during (i-iii) must be less than ϵ.

We dub such many body systems informational active matter and derive their phenomenological properties from microscopic control actions using kinetic theory and information theoretic arguments.

* vitelli@uchicago.edu

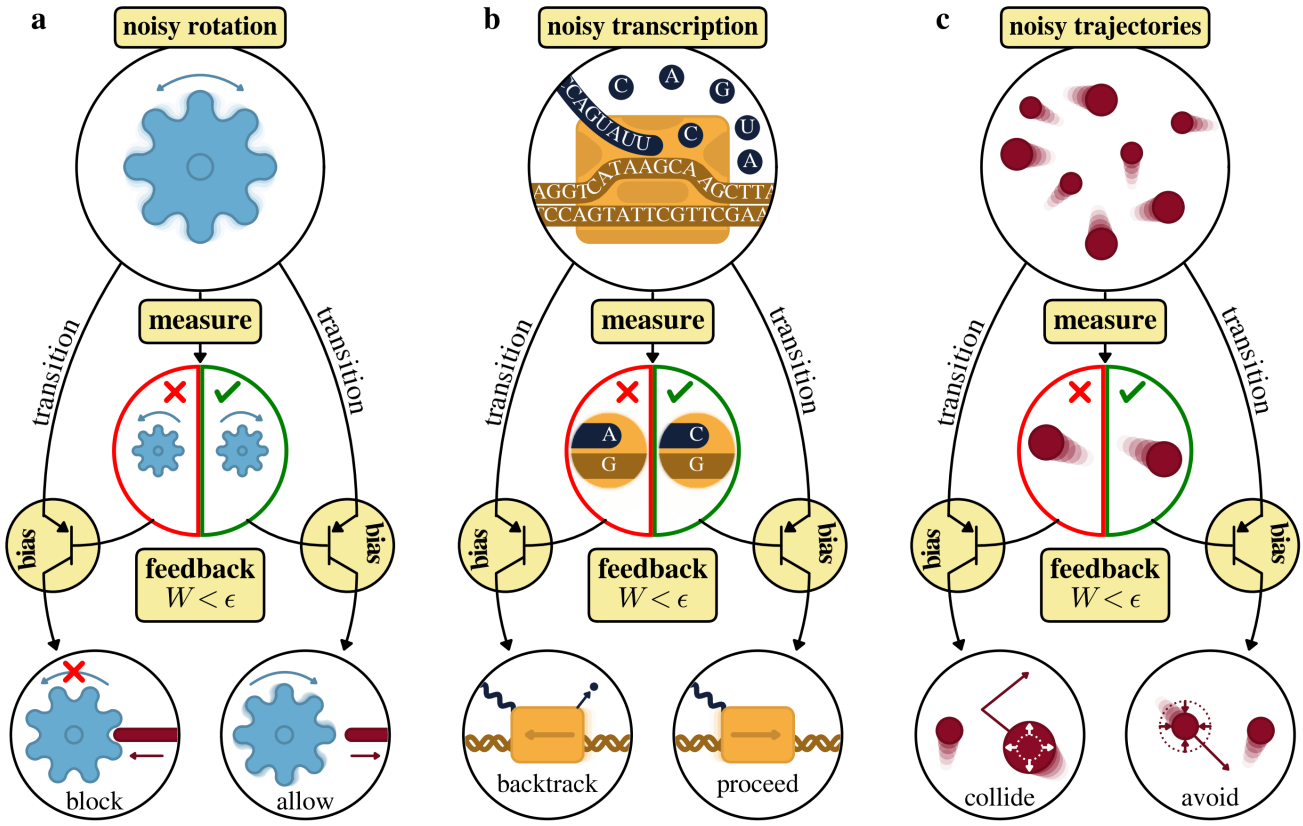

FIG. 1. **Information ratchets in biology and active matter.** **a** Schematic representation of an information ratchet process. After measuring the fluctuating forces on the ratchet, a pawl is selectively inserted (withdrawn) to block (allow) counterclockwise (clockwise) rotations. With sufficient finesse, inserting the pawl requires negligible work; this engine converts noise and information to biased rotation. **b** The action of an RNA polymerase protein, viewed as an information ratchet that converts noise and information into correct RNA sequences. This protein builds an RNA strand (blue) from a DNA template (brown). Bases are added to the growing strand stochastically. When an incorrect base is randomly added, a 'backtracking' procedure is triggered that reverses the motion of the protein and ejects the incorrect base. **c** The thinker gas model of a material built from information ratchets. Agents are particles that measure their position, velocity, and the presence of nearby particles. This information is used to selectively avoid or enhance collisions by changing particle diameters. This distributed engine converts noise and information into coordinated many-body motion, as explored below.

The thinker fluid. We illustrate this general approach using a minimal model: a fluid comprised of 'thinker' particles (Fig. 1c). Each thinker particle is a freely moving hard disk within a gas agitated by noise. Thinkers are able to measure their location, velocity, and the presence of nearby particles (property i). They can also selectively change their diameter, influencing the likelihood of collision with other particles (property ii). Crucially, diameter changes are made according to the outcome of measurements, creating a feedback loop (property iii). The choice of a diameter change as the controlled property, rather than a change in self-propulsive force or direction is not accidental. It is one of simplest ways to directly change how agents interact (during collisions) which allows us to focus on the emergence of simple forms of collective (or social) behavior. If the diameter change is restricted to periods between collisions, then thinkers need only exert a negligible amount of work (ϵ) to control their scattering transitions (property iv). As $\epsilon \to 0$ this system can be viewed as a fluid of Maxwell demons (i.e. microscopic controllers) that redistribute particle density over volumes of phase space by biasing scattering events throughout the system in order to extract work. This minimal model generalizes single-demon devices such as the Szilard engine and provides glimpses in the emergent behavior of more realistic ensembles of informational ratchets, while remaining mathematically tractable.

An example of a simple diameter change rule is shown in Fig. 2a, where agents adopt a small diameter (D_s) when traveling right, and a large diameter (D_l) when traveling left. Obeying the bound set by $\epsilon = 0$ requires prohibiting diameter expansions that cause overlaps (Fig. 2b, dashed outline). Coupling velocity to diameter changes as in Fig. 2a generically breaks detailed balance, which can be seen by comparing a forward and reverse collision process (Fig. 2c-d). After a collision modifies an agent's velocity ($\vec{v} \to \vec{v}'$) a 'reverse' collision beginning from velocity $-\vec{v}'$ will not recover the initial configuration if a diameter change has also oc-

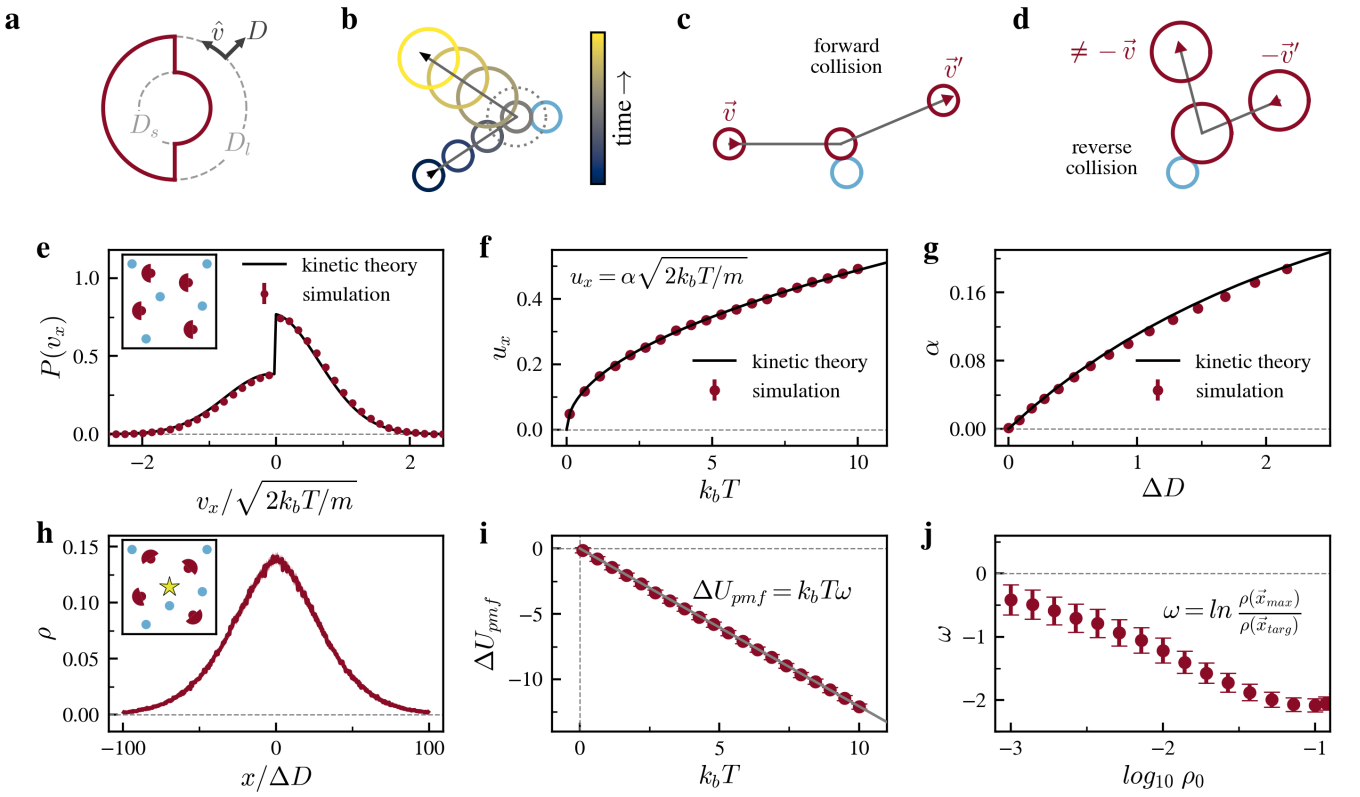

FIG. 2. **The thinker gas biases collisions to produce flows.** **a** A simple discrete diameter rule for a thinker particle. Thinkers traveling right (left) adopt small (large) diameters. **b** Collision of a thinker with diameter rule **a** and an immobile object (blue disk). Diameter changes are prohibited when overlaps would occur (dashed outline). **c** A forward collision between a thinker with diameter rule **a** and an immobile obstacle (blue disk). Thinker velocity is transformed from $\vec{v}$ to $\vec{v}'$. **d** The reverse process to **c**. Because of the diameter change, the collision starting from thinker velocity $-\vec{v}'$ does not return to $-\vec{v}$, indicating broken detailed balance. **e** Velocity distribution function of a 2D isothermal simulation of thinkers (with diameter rule shown in **a**) immersed in a passive hard-disk gas. Thinkers are concentrated in the positive half of the velocity plane, as predicted by a kinetic theory developed below. **f** Mean bulk velocity u_x of thinkers in **e** as a function of temperature, with fixed $\Delta D = 1$. Mean bulk flow due to collisional biasing is a fraction α of the thermal speed, where α is not a function of temperature. **g** Ratio of mean bulk velocity to thermal speed as a function of diameter change for thinkers in **e**. **h** Positional distribution function in x for a 2D isothermal simulation of thinkers that choose a small (large) diameter when moving towards (away) from a fixed reference point (indicated by a star at the origin), immersed in a passive gas. Thinkers are concentrated near the target location. **i** Depth of an effective potential consistent with the increased density of thinkers near the target in **h**, as a function of temperature. Effective potential depth is ωk_bT, where ω is not a function of temperature. **j** Ratio of the effective potential depth and temperature for thinkers in **h** as a function of initial total density ρ_0

curred. We demonstrate the consequences of this broken collision microreversibility through a molecular dynamics (MD) implementation of the thinker gas (in the package `HOOMD-Blue` v2.9.3 [50], see methods).

Active driving from local measurements. Figure 2e shows the results of a simulation of thinkers held at constant temperature, with the diameter coupling shown in Fig. 2a and immersed in a fixed-diameter gas. The resulting velocity probability distribution is not Gaussian: thinker velocities are concentrated along the positive-x direction, as they are more likely to enter regions of phase space with smaller scattering cross-sections. This departure from the Maxwell-Boltzmann (MB) distribution occurs despite energy and momentum conservation (to algorithmic precision) in the molecular dynamics simulation (see SI Figure S1), and while undergoing collisions with a passive, MB-distributed gas. Such asymmetric distributions have non-zero mean velocity, as revealed by computing the first moment, $u_x = \int v_x P(v_x) d\vec{v}$, as shown in Fig. 2f. This mean velocity is $u_x = \alpha\sqrt{2k_bT/m}$, a fraction ($\alpha < 1$) of the thermal speed for particles of mass m at temperature T. The quantity α is a temperature-independent function of the change of thinker diameter ($\Delta D = D_l - D_s$, Fig. 2g). The shape of the velocity distribution, mean velocity, and temperature-independent driving strength α obtained from microscopic simulations (red data in Fig. 2e-g) can all be predicted to high accuracy using a kinetic theory of the thinker gas (black curves), which we will describe in detail later.

A more complex diameter rule is shown in Fig. 2h, where agents have diameters coupled to both velocity

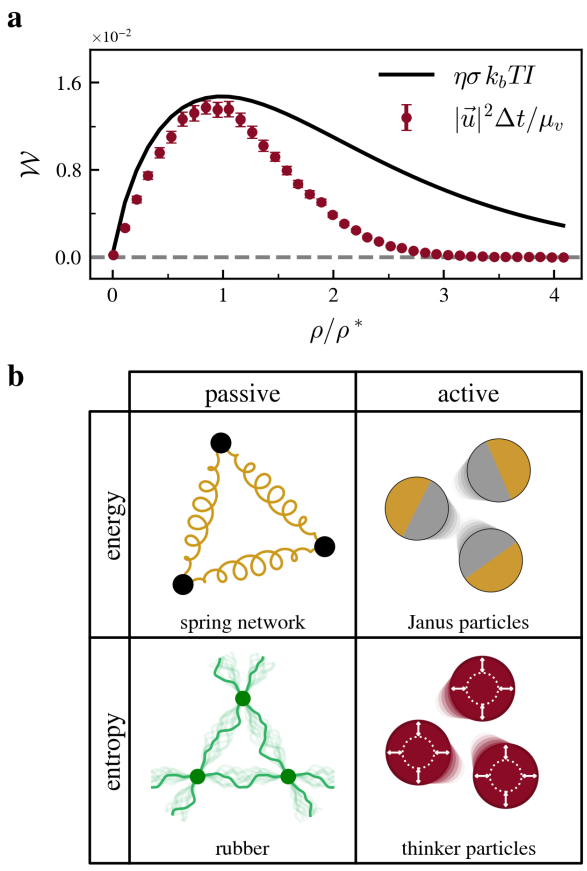

FIG. 3. **The thinker gas as entropic active matter.** **a** Work done to propel a thinker through a passive gas per measurement cycle (duration Δt). Power dissipated in thinker propulsion is estimated from simulation by finding the density-dependent drift velocity $\vec{u}$ and mobility coefficient μ_v. The black curve is the average free energy dissipated in deleting the thinker's memory of prior measurements, obtained from a Markov chain model of the thinker measurement process (see methods and extended Fig. E1), where σ is the intrinsic efficiency of rectification by collisional biasing and η is a fitted constant of order one. **b** Conceptual categories of mechanical media. Spring networks at low temperature are equilibrium (i.e. passive) media with properties dominated by internal energy (upper left). Rubber-like materials at finite temperature are also in equilibrium, but have a mechanical response dominated by the entropy of available chain conformations (lower left). Non-equilibrium, or active, media driven by mechanical work include Janus particles, submicron rocket-like devices that consume a chemical fuel (upper right). Thinker particles complete the table as a non-equilibrium material with properties controlled by measurement and feedback; essentially entropic processes (lower right).

and position - when moving towards (away from) a fixed reference point, a small (large) diameter is chosen. Intuitively, an initially homogeneous spatial distribution of agents densifies near the reference point. When viewed without knowledge of the diameter change process, one might think that this isothermal thinker gas is in a potential well centered on the reference point. A potential consistent with this observation can be found by computing the potential of mean force defined as $U_{pmf}(\vec{x}) = -k_bTln\rho(\vec{x})/\rho_0$, which assumes that the likelihood of observing a density configuration $\rho(\vec{x})$ is Boltzmann distributed according to a free energy $U_{pmf}(\vec{x})$ [51]. The depth ΔU_{pmf} of this effective potential scales linearly with temperature (Fig. 2i), indicating that the high density of thinkers near the target location is in fact independent of temperature, unlike the case for an externally applied energetic potential, where increased temperature allows particles to escape confinement. The logarithm of the relative density of thinkers near the target, $\omega = ln\ \rho(\vec{x}_{max})/\rho(\vec{x}_{targ})$, shown in Fig. 2j, increases with increasing initial total gas density ρ_0.

Information-theoretic arguments. Recall that a Szilard engine can lift an external load as long as information is not erased from the memory of the controller (i.e. demon) needed to operate it [19]. Similarly, thinker particles can extract the work needed to propel themselves through a surrounding gas with speed u from the gas itself, solely by performing measurements and control actions. The work needed is $\mathcal{W} = u^2\Delta t/\mu_v$ where μ_v is the particle mobility and Δt is the time between measurements. According to Landauer's principle, the amount of work extracted is bounded by

$$\mathcal{W} \leq k_bTI, \tag{1}$$

the energy needed to erase the information I collected during such measurements [17, 19, 52–55]. we shall assume for simplicity that the thinkers are not allowed to do any mechanical work W to expand, i.e. $\epsilon = 0$.

We first provide a qualitative argument for the dependence of $\mathcal{W}$ on density. Information is encoded in the binary diameter state of the thinker particle. At low density, negligible information (and hence $\mathcal{W}$) is gained because collisions are so rare that thinker velocity (and hence diameter) is nearly constant. Collision frequency (and also information acquired) increases with ρ, up until a characteristic density $\rho^* \sim 1/A(\Delta D)$, where $A(\Delta D)$ is the area of the annulus defined by the excluded area change of a thinker whose diameter expands by ΔD. Crucially, expansion of a thinker reduces the phase-space volume available to the surrounding gas by the amount $A(\Delta D)$. Above ρ^*, thinkers are nearly always crowded by other particles and hence forbidden from changing their diameter. Assuming that particles are distributed over space uniformly, we can use a Poisson distribution to estimate the probability of a successful expansion as $e^{-\rho/\rho^*}$. Information and work are therefore exponentially suppressed in the large ρ limit.

To estimate the average information gained by measurement, I (and hence the maximum $\mathcal{W}$ in Eq. 1), we construct a two-state Markov chain model for the binary diameter change process (see methods and extended Fig. E1). The mean information (or entropy, for error-free measurements) of a Markov chain at steady state per

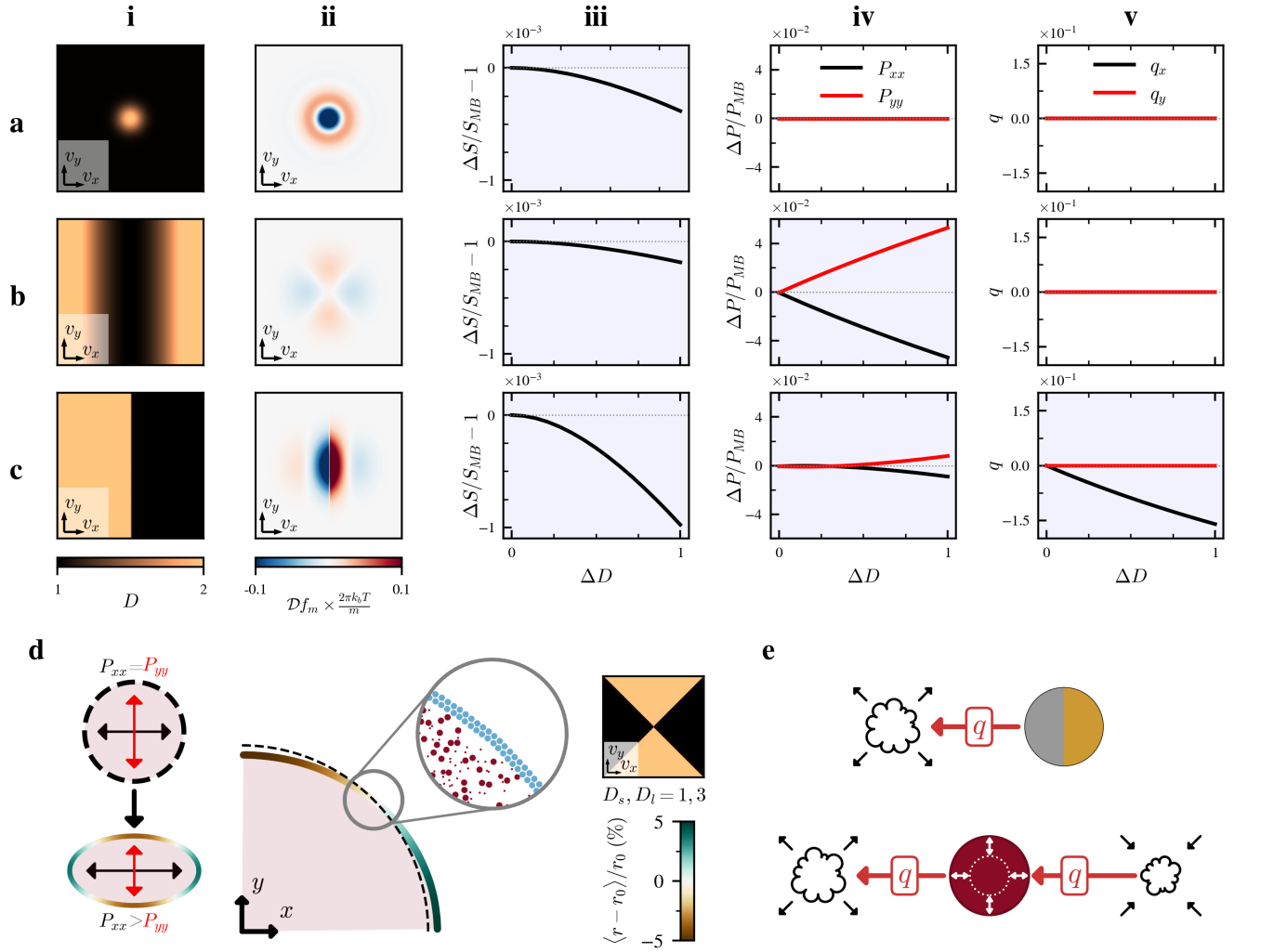

FIG. 4. **Observable consequences of thinker measurements.** Kinetic theory of the thinker gas reveals collective properties. **i** Diameter in the velocity plane, **ii** deviation from the Maxwell-Boltzmann (MB) distribution, **iii** distribution entropy ($S = \int f_t \, ln \, f_t d\vec{v}$) relative to the MB distribution, **iv** pressure ($P_{ij} = \rho m \int v_i v_j f_t d\vec{v}$) relative to the MB distribution, and **v** heat flux ($q_i = (\rho m/2) \int v_i |\vec{v}|^2 f_t d\vec{v}$) for **a** a radially symmetric Gaussian diameter function, **b** an anisotropic quadratic function, and **c** a step function. **d** A thinker gas with an anisotropic diameter function in a flexible container. Diameter function anisotropy produces an anisotropic pressure tensor, deforming an initially circular passive container into an ellipse. **e** Comparison of worker and thinker type propulsion, by analogy to rockets. In the case of a Janus particle (top), heat from burning a fuel is directed backwards, into expanding exhaust which does work on its environment; a propulsive force results as for a macroscopic rocket. Consider a 'thinker' rocket (bottom) in which the expansion of exhaust behind is paired always with a contraction ahead, exactly canceling the work of expansion. This would however require the flow of heat from front to back (and cold to hot), necessitating entropy production.

step is [53, 55, 56]:

$$I = -\sum_{ij} \mu_i P_{ij} \; ln \; P_{ij}. \tag{2}$$

where P_{ij} are the transition probabilities between discrete states occupied with probability μ_i. Note that this entropy is distinct from the entropy production rate often discussed in the stochastic thermodynamics of active systems [57, 58], which is zero because there are only two states corresponding to the binary diameter choices of a thinker particle moving through a passive isothermal gas. These diameter states encode the outcome of local measurements. Combining Eqs. 1 and 2 we obtain an estimate of the maximum work extracted $\mathcal{W} \approx \eta \sigma k_b T I$, where σ is a rectification efficiency for hard disk collisions (see methods) and η is a fitting parameter of order one. Our estimate for $\mathcal{W}$, plotted in Fig. 3a (black curve), qualitatively captures the trend observed in MD simulations (red symbols), as well as our intuitive argument for the dependence of $\mathcal{W}$ on ρ.

The thinker-gas example underscores the general point made in the introduction, namely that informational active matter is in a distinct category from energy-driven active matter (e.g. autophoretic colloids [34]), because it derives its activity by harnessing information (i.e. entropy) and noise. With its ability to break detailed bal-

ance, it is a non-equilibrium counterpart to entropic passive matter [42, 59] such as rubber, which has mechanical properties that also scale with noise. The thinker gas (and the larger category it exemplifies), completes the simple taxonomy of active/passive, energetic/entropic systems (Fig. 3b).

Kinetic theory: compressible phase-space flows. We now sketch how kinetic theory yields an accurate prediction for the thinker self-propulsion speed, and more generally collective properties of informational active matter, such as pressure or heat flux, starting from the microscopic agent strategy. Consider the force-free and spatially homogeneous Boltzmann equation,

$$\frac{\partial f}{\partial t} = \mathcal{Q}(f) \tag{3}$$

where $\mathcal{Q}$ is the collision operator, which describes the manner in which particle collisions redistribute probability density in phase space, and $f(\vec{v}, t)$ is a single particle velocity distribution function. The collision operator here will be modified from its usual form to include the feedback process in Fig. 1c, which measures particle velocities (property i) and promotes or suppresses scattering transitions (property ii) in a feedback loop (property iii), all subject to a work bound (property iv). Scattering events are modeled using the quadratic collision operator [60]:

$$\mathcal{Q} = \frac{1}{2}\int\int B(\sigma, \Delta\vec{v}) \left[\beta f(\vec{v'}) f(\vec{v'}_*) - f(\vec{v}) f(\vec{v}_*)\right] d\sigma d\vec{v}_* \tag{4}$$

where $\vec{v}$ and $\vec{v}_*$ are the velocities of particles undergoing collision, and $\vec{v}'$ and $\vec{v}'_*$ are their post-collision velocities. The collision kernel B describes the scattering of particles for a given impact parameter σ. Crucially, the function β weights the post-collision joint probabilities relative to the pre-collision ones and it is always equal to one if detailed balance (i.e. microscopic reversibility) holds. When $\beta = 1$, the steady-state solution of Eq. 3 is the Maxwell-Boltzmann (MB) velocity distribution for fixed diameter particles. This is not the case in informational active matter (see Fig. 2e for an example), where β is generically a function of measured microscopic properties of the system, e.g. velocities. The feedback control strategies that bias the relative likelihood of transitions between states introduce distortions of phase space represented by a $\beta(\vec{v}, \vec{v}', \vec{v}_*, \vec{v}'_*) \neq 1$ term. Dissipation in granular media [61] or mechanical self-propulsion in flocking media [62] can also introduce such compressible phase space flows but for informational active matter $\beta \neq 1$ even if collisions still conserve energy and momentum (i.e. $\epsilon = 0$).

Diameter change strategy and phase-space distortion. For the thinker gas, the collision operator should describe the evolution of a variable-diameter hard disk gas. Therefore the collision kernel B takes on the form for hard disk collisions (See S.I. section S4.2), while β is a ratio of collision cross sections before and after the collision. For situations in which thinkers predominantly interact with a surrounding, fixed diameter gas (as in Fig. 2), β can be shown to have the form (see methods):

$$\beta = \frac{D(\vec{v}') + D_{fix}}{D(\vec{v}) + D_{fix}} \tag{5}$$

where D is a function describing the diameter of thinkers in velocity space, D_{fix} is the diameter of the passive species, and the passive species has been arbitrarily assigned to starred velocity variables. For pure thinker gasses (see SI), D_{fix} should be replaced with functions of $\vec{v}_*$ and $\vec{v}'_*$. Using this form of the collision operator, a single-particle distribution function f_t can be found that is the steady state solution for the variable-diameter gas. This solution f_t is a distribution that can be decomposed as $f_t = (1 + \mathcal{D}) f_m$, where $\mathcal{D}$ is a function of velocity and f_m is the MB distribution. In a dilute gas with $\beta = 1$, the MB distribution is prescribed by quantities conserved during particle collisions (i.e. particle number, momenta, and kinetic energy). The same constraints apply to the thinker gas by construction (as $\epsilon = 0$), and therefore the zeroth, first, and second order moments of its distribution must be equal to their MB counterparts. This relation defines a sufficient set of constraining equations to solve for f_t explicitly (see methods).

Kinetic theory and symmetries of the feedback control strategy. Symmetries of the microscopic constituents are crucial in determining material properties, and informational active matter is no exception. In this case, the symmetries of the feedback control strategy directly set which macroscopic properties of the active gas depart from the passive MB distribution. We demonstrate this using the thinker gas operating with several strategies for $D(\vec{v})$ (Fig. 4a-c). Isotropic diameter functions (Fig. 4ai) lower the gas entropy (Fig. 4aiii), but have no consequences on gas pressure (Fig. 4aiv) or heat flux (Fig. 4av). Anisotropic diameter functions with reflection symmetry impact the entropy of the distribution and pressure, but not the heat flux (Fig. 4bi-bv). When a thinker gas with an anisotropic microscopic feedback strategy (and therefore an anisotropic pressure) is confined within a flexible, initially-circular container, deformation into an ellipse results (Fig. 4d).

Diameter functions that lack reflection symmetry modify entropy, pressure, and the heat flux vector $\vec{q}$ (Fig. 4ci-cv). A non-zero heat flux is responsible for the striking propulsive effects demonstrated in Fig. 2. The velocity distribution of thinkers in Fig. 2e (as well as pure thinker gases, see extended Fig. E2) can be accurately predicted from our kinetic theory, including the mean propulsion speed shown in Fig. 2g. Assuming that thinker bulk motion accounts for the entirety of energy flux in the system, i.e. $\vec{q}/\rho + k_b T \vec{u} = 0$, the self propulsion speed is

$$u_i = -\frac{m}{2k_b T}\int v_i |\vec{v}|^2 f_t d\vec{v}. \tag{6}$$

For mechanically active systems, the propulsive consequences of heat flux are familiar: Janus particles, much

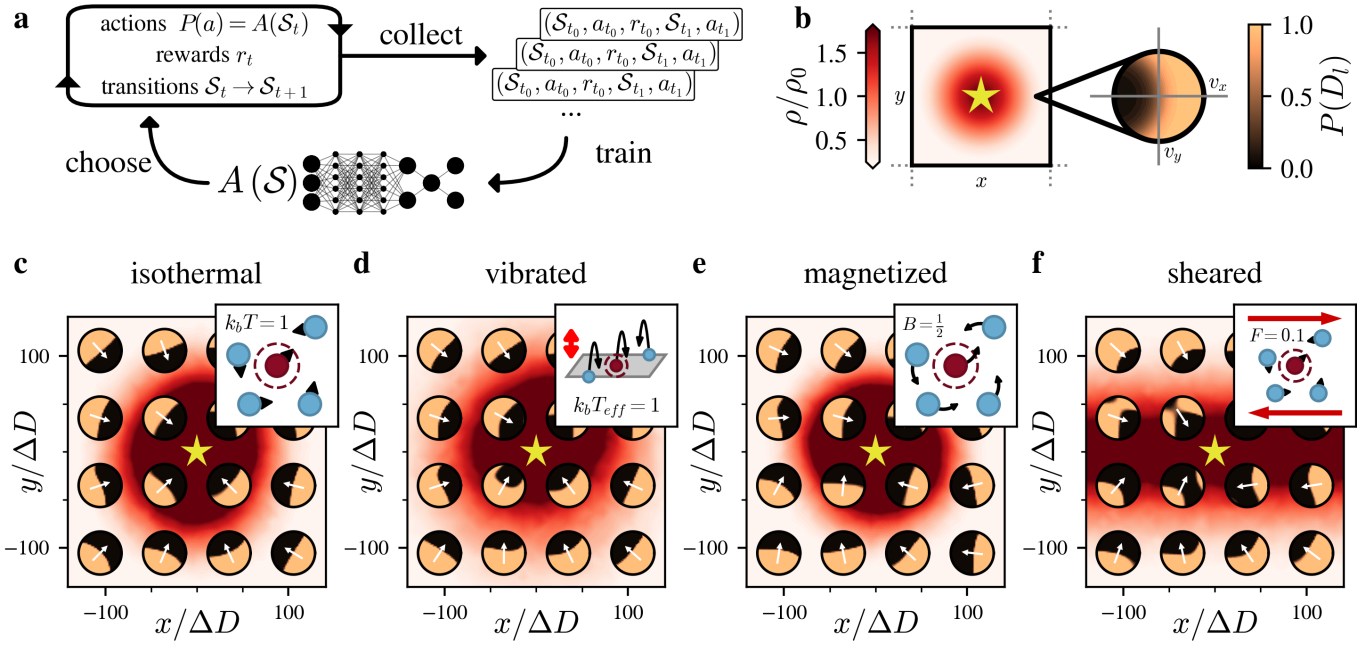

FIG. 5. **Thinker self-propulsion strategies and reinforcement learning. a** The RL learning cycle. Actions are chosen according to a policy function, and experiences of transitions are accumulated in a buffer. This buffer is used to train a feed-forward artificial neural network that defines the policy function. **b** Locomotion task definition and legend. Agents are embedded in a periodic environment with a singly-peaked (indicated by star) reward function. Agent density after learning is shown in red. The RL algorithm searches for a probabilistic discrete diameter function of $\vec{v}, \vec{x}$ that most rapidly moves agents towards the maximum. Plots in **c-f** follow the same color scheme. **c-f** RL diameter functions under various transport physics. **c** Isothermal environment. **d** Vibrated granular bed environment. **e** Isothermal dynamics with applied magnetic field. **f** Langevin dynamics with applied shear field. In all cases, the vector field found by odd moments over the learned diameter distribution ($\vec{\xi}$) points along the shortest-time path towards the reward maximum (white arrows).

like rockets, move by transferring heat backwards to their expanding exhaust products (Fig. 4e, top). However for informational active matter, exemplified by the thinker gas, no analog of the combustible fuel is present. Heat is taken from the surrounding medium instead and directed backwards using on-board information processing (Fig. 4e, bottom).

Reinforcement learning: self-propulsion strategies for non-thermal noisy environments. Our kinetic theory applies in the dilute, spatially homogeneous regime when the noise is thermal. But how can we proceed at high densities or in more general chaotic environments such as turbulent or non-thermally driven fluids? Reinforcement learning (RL), a trial-and-error process whereby agents learn to maximize rewards supplied by an environment (Fig. 5a) [63–69], provides an agnostic method to search for transition-bias strategies in regimes beyond the reach of our kinetic theory. Again, we employ the thinker gas as our test system of choice, and seek to agnostically learn a diameter (i.e. transition-biasing) strategy $D(\vec{x}, \vec{v})$. Standard techniques from the field of policy optimization [70] (see methods) are used to train a single-particle probabilistic discrete diameter function ($P_{D_l} = 1 - P_{D_s}$) of position and velocity that climbs a singly-peaked 'reward' function in the shortest possible time (Fig. 5b).

This locomotion task is solved by self-propulsion along the least-time path from anywhere in the simulated domain to the most-rewarded point. Thinker agents may experience various fluctuating forces, but ultimately only those that persist after long time averaging (i.e. external forces) are important to the geometry of least-time paths. We can reveal this from RL-learned diameter functions by taking an odd moment over the probability of choosing a large diameter, P_{D_l}:

$$\xi_i(\vec{x}) = -\int v_i P_{D_l}(\vec{x}, \vec{v}) d\vec{v}. \tag{7}$$

where the biasing vector field $\vec{\xi}$ is the direction of greatest reflection asymmetry for the learned diameter strategy, which we expect from kinetic theory to be parallel to the direction of greatest heat flux, and therefore also propulsion. Figure 5c-f illustrates how agents learn to navigate four different mixtures of thinkers and passive agents: a 2D thermostat-coupled periodic domain, a 3D vertically agitated (i.e. a granular bed) domain, a 2D thermal gas with applied magnetic field, and a 2D dissipative gas with applied shear field (See methods for numerical details). The biasing vector field $\vec{\xi}$ (shown as white arrows) adopts a simple geometry pointing towards the most-rewarded point (i.e. $\vec{\xi} = -\hat{x}$ for targets at the origin), regardless of the type of agitating noise (even when this noise is the result of non-conservative collisions, see extended Fig. E3).

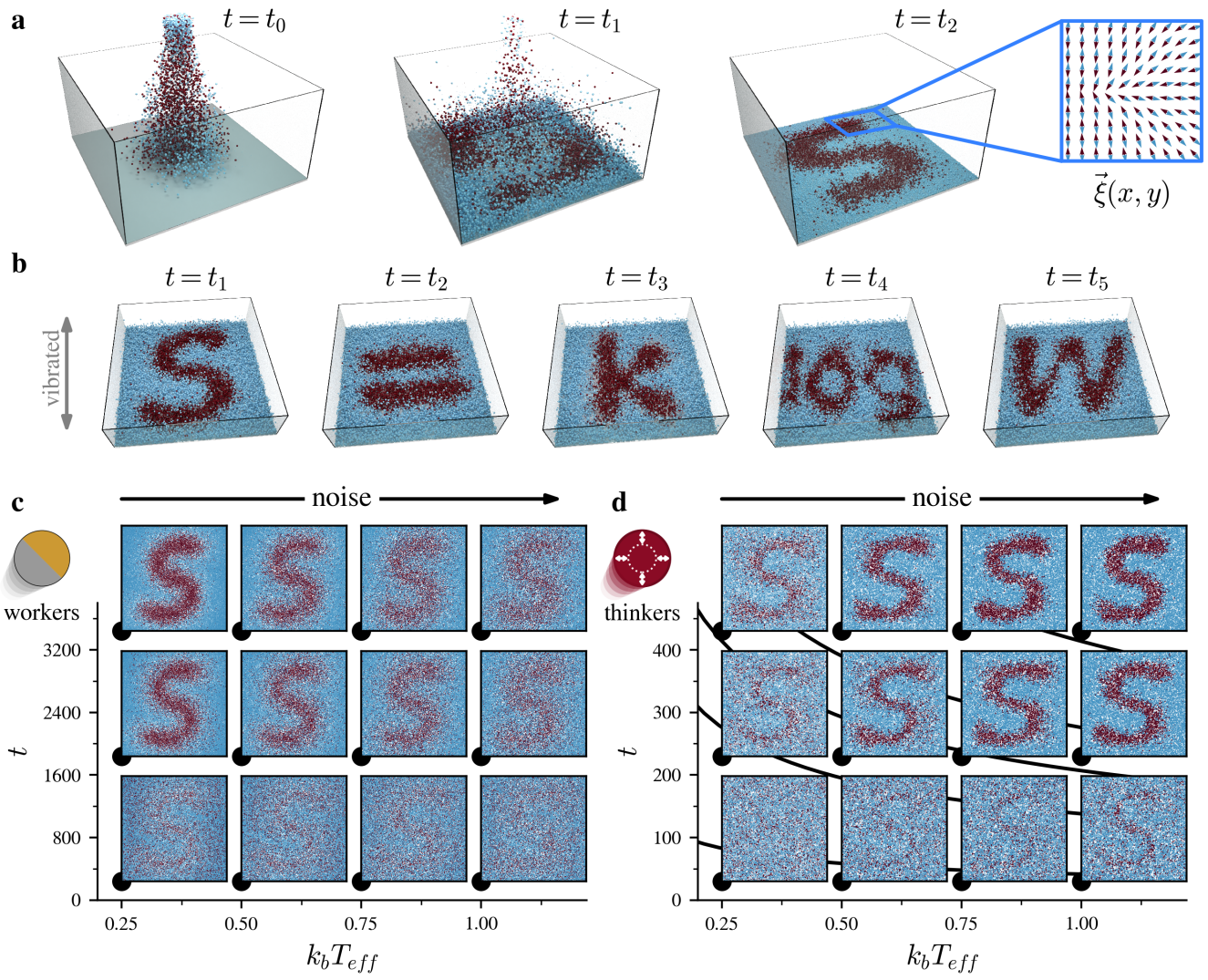

FIG. 6. **Noise-driven active patterning.** **a** A collection of variable-diameter particles are dropped into a hard-sided box. As particles undergo elastic collisions, their velocities are reduced by a linear drag term and they settle onto the bottom of the box. The two species (red and blue) have opposite $\vec{\xi}(\vec{x})$ fields (inset), driving strong separation into a designed pattern. **b** Patterns can also be formed in continuously vibrated beds. Here, Boltzmann's classic equation is written frame-by-frame while thinkers are agitated by a correlated noise source, approximating a vertical shaker table. **c** Worker (self-propelled) particles that exert a constant force in the direction specified by $\vec{\xi}$, constantly agitated as in **b**. As in **a**-**b**, red and blue particles move in opposite directions on the same $\vec{\xi}$ field. As agitation is increased (k_bT_{eff}), pattern resolution degrades, since particles can only push with a fixed amount of force. Frames are instantaneous snapshots of simulations at the time and effective temperature indicated by the position of the inset lower left corner. **d** Thinker particles following the diameter rule of eq. 8 and the same $\vec{\xi}$ field and athermal agitation as **c**. The time required to obtain a given letter resolution decreases with increasing agitation, demonstrating the temperature dependence of informational active driving. Black curves are $t = sL/\sqrt{2mk_bT_{eff}}$ for $s = 0.15 \to 2$ where L is the size of the simulation domain.

The biasing field only changes in response to external forces such as the magnetic field in Fig. 5e (which causes $\vec{\xi}$ to spiral about the target) or shear field in Fig. 5f. Also notice that the learned probabilistic diameter functions are well-approximated by the deterministic strategy:

$$D(\vec{x}, \vec{v}) = D_s + \Delta D \mathbb{H}\left(-\vec{v} \cdot \vec{\xi}(\vec{x})\right) \tag{8}$$

where $\mathbb{H}$ is the Heaviside step function. We now demonstrate how to design a self-generated flow of thinkers in any noisy environment, (even environments of other thinker species) using a chosen biasing field $\vec{\xi}(\vec{x})$ and eq. 8 as the feedback protocol.

Information landscapes and noise-driven active patterning. When the transition-biasing strategy of informational active agents is spatially dependent, it effectively creates an *entropically*-derived free-energy landscape. To illustrate this point, we design bias fields to produce a pattern formed by two species of thinker par-

ticles (in three dimensions) dropped from a hopper onto a surface (Fig. 6a). Energy is dissipated via linear drag, eventually resulting in a stationary layer. By choosing the bias field for each species, complex patterns can be formed from this apparently chaotic process. Note that gravity and interactions with the smooth container walls are the only potential energy fields acting on particles - patterns arise entirely from the biasing of collisions. Furthermore, the bias field can also be a function of time, $\vec{\xi}(\vec{x},t)$. Figure 6b shows thinkers continuously agitated by correlated noise (approximating a shaker table). Rather than following a fixed biasing field, thinkers switch target configurations so as to write out Boltzmann's entropy equation (See electronic S.I. for videos of these processes). Note that unlike a similar pattern formed by an externally applied potential, thinkers define their pattern by the bias field which is carried on board the collective. Thinkers with the capacity to form a single pattern need only be given a slightly different instruction set to form any other pattern (or sequence of patterns) with similar resolution.

Entropically-derived free-energy landscapes exhibit a striking difference from their energetic counterparts: their depth is controlled by the level of noise. We highlight this phenomenon by contrasting pattern formation by self-propelled worker and thinker particles. Two species of worker particles (red and blue) that exert a constant-magnitude force driving them oppositely along the direction of a bias field will phase separate (Fig. 6c), producing an effect equivalent to an external potential field. However as agitation (approximating a shaker table, and resulting in a mean per particle kinetic energy of k_bT_{eff}) is increased, pattern resolution drops as worker effort is overwhelmed by noise. In contrast, the infinite-time resolution of thinker particles experiencing the same agitation is not affected by the strength of the noise (see Fig. 2e for the thermal case), as informational driving grows with fluctuations. In fact, the finite-time resolution of these patterns is set by propulsion speed, which for thinker particles increases with temperature (Fig. 2b). For a finite time, increasing k_bT_{eff} actually increases the resolution achieved by thinkers (Fig. 6d), completely at odds with the trend for workers under the same conditions. Notice also that when random fluctuating forces are comparable to the magnitude of worker driving (as in Fig. 6c), the long-distance transport speed for workers is significantly slower than that for thinkers. Workers must exert large forces to drive themselves rapidly through a fluid, as collisions continually redistribute applied work into random motion. Conversely, thinkers harness random motion into a drift velocity that is on the order of the mean thermal speed.

Informationally active agents can exploit chaotic, non-steady environments to form complex patterns by redistributing (through measurements) the flow of energy between their degrees of freedom. While we have emphasized the limiting case where informational driving dominates, our results may shed light also on more realistic situations where mechanical and informational active processes coexist. For example, cells living in crowded conditions must make decisions to change or maintain their diameter, sometimes in response to external cues [71–73]. Such actions have constrained metabolic costs (property iv). In addition, they alter the mechanical and chemical interaction cross section with their similarly changing neighbors (properties i-iii). As miniaturized robots cross the cellular length scale [14] they must contend with omnipresent thermal fluctuations, and also intense non-thermal fluctuating forces in some environments (e.g. the human circulatory system). Our work offers an organizing principle to understand when and how such small intelligent agents can exploit, rather than fight, their noisy environment.

METHODS

Microscopic model implementation. Molecular Dynamics (MD) simulations of the thinker gas were performed with the open-source software package `HOOMD-Blue` (v2.9.3) [50]. The package was modified with a custom updater that performed the following actions on each thinker particle every fixed interval of timesteps:

1. Find neighbors (of any type, including passive particles in the environment) within a distance of 1.5 times the maximum interaction cutoff distance. Find the minimum distance between the particle center and the boundary of a neighbor particle ($r^n_{min} = r_{ij} - D_j/2$).
2. Evaluate a function $D(\vec{x},\vec{v})$ which determined the desired new diameter of the particle (D_{new})
3. Change particle diameter.
   (a) $D_{new} > D_{old}$ and $D_{new}/2 > r^n_{min}$. Expansion would cause particle overlap. The diameter change is discarded.
   (b) $D_{new} < D_{old}$ and $D_{old}/2 > r^n_{min}$. This particle is currently interacting with a neighbor. Reducing its diameter would cause a potential energy change. The diameter change is discarded.
   (c) $D_{old}/2 < r^n_{min}$ and $D_{new}/2 < r^n_{min}$. No overlaps will be added or removed by the diameter change, and it proceeds.

This sequence of steps is done in series for all thinker particles so as to avoid a race condition which would change the value of r^n_{min}. All particles interact through a shifted Weeks-Chandler-Andersen potential (sWCA) [74], where the origin is shifted so that the radius of the particle is the potential's zero isoenergy surface. This potential (implemented in the function `hoomd.md.pair.slj`) takes the form:

$$V_{\mathrm{sWCA}}(r) = 4\varepsilon\left[\left(\frac{\sigma}{r-\Delta}\right)^{12} - \left(\frac{\sigma}{r-\Delta}\right)^{6}\right] + \varepsilon$$

for $r < (r_{cut} + \Delta)$ and $V_{sWCA} = 0$ otherwise, where $\Delta = (D_i + D_j)/2$ and D_i, D_j are the diameters of the interacting pair. The radial shifting was chosen with $\sigma = 0.5$ so that the minimum (located at $\sigma 2^{1/6}$ in the unshifted case) is at a distance of $D_0 = 2^{1/6}$. This sets the value of r_{cut} in the interaction potential to $\sigma 2^{1/6}$. The depth of the attractive well was set to $\varepsilon = 1$. Isothermal simulations in Fig. 2 were carried out with a velocity Verlet integration and a Nosé-Hoover thermostat, as implemented in `HOOMD-blue`. System thermal energy was held at $k_bT/\varepsilon = 1$, and particle mass was fixed at $m = 1$ (in simulation units). Constant-energy simulations confirmed that the diameter change protocol outlined above does not contribute to internal energy drift of the ensemble (see SI section S2) during numerical integration.

Simulations of thinker gases contained in flexible containers (Fig. 4e) were conducted using constant-energy Verlet integration of the gas and Langevin integration of the flexible container ($k_bT = 1$, damping parameter $\gamma = 2$). The container consisted of two close-packed layers of beads with diameter D_l, bonded to nearest neighbors by harmonic springs of stiffness $k = 100$.

Thinker Markov model. The information gained by a thinker particle immersed in a passive gas can be estimated from a Markov chain model, as referenced in Fig. 3a. The model is constructed by first considering the diameter transitions that depend upon gas collisions and crowding, shown schematically in extended Fig. E1a. Thinkers undergo random collision with the passive surrounding gas, with probability P_{coll}, which then randomizes their velocities into the forward or reverse velocity half spaces with probabilities P_+ and P_-, respectively. If a thinker's velocity is such that a diameter expansion is attempted, no nearby particles must obstruct the expansion. The probability that this requirement is met is denoted by $P_<$, i.e. if an overlap is created the work exerted by the thinkers must be less than the value ϵ, which can be set to zero if desired. The transition diagram can be condensed into a binary model of the form shown in Fig. E1b. We utilized several elementary kinetic approximations to define the terms P_+, P_-, P_{coll}, and $P_<$. Velocities are assumed to be randomly re-distributed by collisions on average, with $P_+ = P_- = 1/2$. We assume a collision timescale for the gas:

$$\tau^i_{coll} = \frac{l^i_{mfp}}{c_{th}} = \frac{1}{\rho_0 \sigma^i_{coll}\sqrt{2k_bT/m}} \tag{9}$$

where superscripts indicate different values for the large and small diameter states, l^i_{mfp} is the mean free path for a gas of density ρ_0, σ^i_{coll} is the collision cross section, and $c_{th} = \sqrt{2k_bT/m}$ is the thermal speed of this isothermal gas. We take the likelihood of a collision having occurred in the time between actions Δt to be

$$P^i_{coll} = 1 - e^{-\Delta t/\tau^i_{coll}}. \tag{10}$$

Assuming that particles are distributed over space uniformly, we can treat their occurrence within an area A as obeying a Poisson distribution, $P(n) = \frac{(\rho A)^n}{n!}e^{-\rho A}$ where n is the number of particles observed and A is the area of the annulus defined by the expanding diameter, $A = ((D_l + D_s)^2/4 - D_s^2)\pi$. This yields:

$$P_< = P(n = 0) = e^{-\rho_0 A}. \tag{11}$$

The stochastic matrix describing this measurement sequence is:

$$\mathbf{P}_{thinker} = \begin{bmatrix} 1 - \frac{1}{2}P^s_{coll}P_< & \frac{1}{2}P^s_{coll}P_< \\ \frac{1}{2}P^l_{coll} & 1 - \frac{1}{2}P^l_{coll} \end{bmatrix}, \tag{12}$$

and the corresponding steady state population is

$$\mu_{thinker} = \begin{bmatrix} \frac{P^l_{coll}}{P^l_{coll}+P^s_{coll}P_<} & \frac{P^s_{coll}P_<}{P^l_{coll}+P^s_{coll}P_<} \end{bmatrix}. \tag{13}$$

For error-free measurements, the information contained in an ensemble of measurements is equal to the Shannon entropy H. For a Markov chain in the steady state, the mean entropy (and therefore information) per step is given by [56]:

$$I(\mathbf{P}) = H(\mathbf{P}) = -\sum_{ij} \mu_i P_{ij}\ ln\ P_{ij}. \tag{14}$$

The Markov estimate of propulsive work $\mathcal{W}$ includes an efficiency term:

$$\sigma = \frac{\tau^s_{coll} - \tau^l_{coll}}{\tau^s_{coll} + \tau^l_{coll}} = \frac{\Delta D}{\Delta D + 4D_0}, \tag{15}$$

which is the ratio of time moving forward over total time, assuming $P_+ = P_- = 1/2$. For the data shown in Fig. 3a, ΔD is fixed and $\sigma = 1/5$, and the fitting parameter $\eta = 5/13$.

Propulsive work was estimated from numerical data by finding the mobility constant from the self-diffusivity of the gas ($\mu_v = D_{self}/k_bT$) for the the given density and temperature conditions. An effective force could then be defined from the drift velocity of the thinker species, $\vec{F}_{eff} = \vec{u}/\mu_v$, and the work per action as $\vec{u} \cdot \vec{F}_{eff}\Delta t$.

Kinetic theory of variable diameter hard disks. We can find the velocities after collision between a pair of hard disks by conservation of momentum and energy. Assuming uniform particle masses, momentum and kinetic energy are conserved through the collision process:

$$\vec{v} + \vec{v}_* = \vec{v}' + \vec{v}'_* \tag{16}$$

$$|\vec{v}|^2 + |\vec{v}_*|^2 = |\vec{v}'|^2 + |\vec{v}'_*|^2 \tag{17}$$

If $\hat{n}$ is a unit vector that points between disk centers at the point of contact (note that $\hat{n}$ therefore depends upon diameter), then the post-collision velocities can be written as (for disks of equal mass):

$$\vec{v}' = \vec{v} - ((\vec{v} - \vec{v}_*) \cdot \hat{n})\hat{n} \tag{18}$$
$$\vec{v}'_* = \vec{v}_* + ((\vec{v} - \vec{v}_*) \cdot \hat{n})\hat{n} \tag{19}$$

For disks of fixed diameter, this scattering process is microreversible; $(\vec{v}, \vec{v}_*)$ maps to $(\vec{v}', \vec{v}'_*)$ and $(-\vec{v}', -\vec{v}'_*)$ maps to $(-\vec{v}, -\vec{v}_*)$, resulting in a Jacobian for the change of variables equal to -1 [75]. This one-to-one mapping allows all four velocity terms to be collected under a common unit disk integration in the typical quadratic Boltzmann collision operator (see supplemental information for additional details). When particle diameters are instead functions of velocity, the microreversibility of the collision process is broken, but can be restored with a shift of relative positions. In a coordinate frame centered on the point of contact for the forward collision, a shift in position of $\beta = (D(\vec{v}') + D(\vec{v}'_*))/(D(\vec{v}) + D(\vec{v}_*))$ along the reflection plane of the forward collision, applied to one particle during the reverse process restores the symmetry of velocity mapping (see extended Fig. E4). Note that when thinker particles are immersed in a fixed-diameter gas, one set of diameters (starred or unstarred) is constant.

We will now solve for the single particle probability distribution function ($f(\vec{v})$) that satisfies the steady state form of eq. 3 for the thinker gas collision operator by examining the collision invariants of the gas. If we consider a moment of the time-varying distribution function $f(\vec{v}, t)$ with a non-time-varying test function ϕ:

$$\langle \phi \rangle_f = \int f(\vec{v}, t)\phi(\vec{v}) d\vec{v} \tag{20}$$

the time evolution of this quantity is:

$$\frac{d}{dt}\langle \phi \rangle_f = \int \phi(\vec{v}) \mathcal{Q}(f)(\vec{v}, t) d\vec{v} \tag{21}$$

The function ϕ can be brought into the integrand of the collision operator since it is not a function of time. As we are now considering an expression integrating over all $\vec{v}$ and $\vec{v}_*$ (and by extension $\vec{v}'$ and $\vec{v}'_*$), the choice of primed and starred variables is entirely arbitrary. A typical procedure is to average over the exchange of velocity variables [75], producing the following for the case of $\beta = 1$:

$$\frac{1}{8}\int\int\int (\phi + \phi_* - \phi' - \phi'_*)\,(f'f'_* - ff_*)\,B(\sigma, \Delta\vec{v}) d\vec{v}_* d\vec{v} d\sigma \tag{22}$$

where B is the collision kernel and σ the impact parameter. If ϕ is a quantity that is conserved through the collision, then it remains unchanged and $\frac{d}{dt}\langle \phi \rangle_f = 0$. This defines a summational collisional invariant for the system. For the Boltzmann equation, summational invariants can only be linear combinations of the microscopically conserved quantities, $\mathcal{M} = 1$, $\vec{v}$, $|\vec{v}|^2$, which are unchanged during collision by construction [76]. Therefore there exist constants $(a, \vec{b}, c)$ that define any summational collision invariant:

$$\mathcal{M}(\vec{v}) = a + \vec{b} \cdot \vec{v} + c|\vec{v}|^2 \tag{23}$$

For the thinker gas with $\beta \neq 1$, the same procedure of exchanging velocity variables allows a common term to be collected, $g = (D_{fix} + D(\vec{v}))\phi$ for the mixed thinker-passive case, or $g = D(\vec{v})\phi$ more generally. This term must satisfy the same condition $g + g_* - g' - g'_* = 0$ for it to remain unchanged by collisions (i.e. be an invariant). We will now define a system of moment equations allowing us to specify the constants that characterize the thinker gas collisional invariant. Beginning with the MB velocity distribution function in 2D:

$$f_m(\vec{v}) = \frac{m\rho}{2\pi kT} e^{-\frac{m|\vec{p}|^2}{2kT}} \tag{24}$$

where $\vec{p} = \vec{v} - \langle \vec{v} \rangle = \vec{v} - \vec{u}$ is the velocity of the gas in the flow frame, we express the thinker gas distribution function as $f_t = (1 + \mathcal{D})f_m$, where $\mathcal{D}$ is a function of velocity only. We can treat the function $(1 + \mathcal{D})$ as a test function operating on the MB distribution, with collisional invariant $g = D(1 + \mathcal{D})$. The four constants a, b_x, b_y, c which define invariant g (and therefore $\mathcal{D}$) can be found by requiring that the first four conserved moments ($\mathcal{M}$) of the thinker gas velocity distribution are equal to the first four moments of the equilibrium MB distribution:

$$\begin{aligned} \int \mathcal{M} f_m d\vec{v} &= \int \mathcal{M}(1 + \mathcal{D}) f_m d\vec{v} \\ 0 &= \int \mathcal{M}\mathcal{D} f_m d\vec{v} \end{aligned} \tag{25}$$

which mathematically states that thinker gases conserve number, momentum, and energy in all collisions, just as the MB distribution. Note that this restriction does not constrain the third-order moments which define the heat flux tensor, or the individual entries of the pressure tensor (derived from second-order moments).

Using the expression for the thinker gas collision invariant, $g = D(1 + \mathcal{D})$, we can trivially reorder to obtain $(1 + \mathcal{D}) = gD^{-1}$. As a scalar function which must be greater than zero, division by D presents no problems (see supplemental information section S4.6). Using this expression for the thinker perturbation, and the notation for expectation value $\langle \phi \rangle_m = \int \phi f_m d\vec{v}$, we can write:

$$\begin{aligned} \langle \mathcal{M} \rangle_m &= \langle \mathcal{M}(1 + \mathcal{D}) \rangle_m \\ &= \langle \mathcal{M} g D^{-1} \rangle_m \\ &= a\langle \mathcal{M} D^{-1} \rangle_m + b_x \langle \mathcal{M} v_x D^{-1} \rangle_m + \\ &\quad b_y \langle \mathcal{M} v_y D^{-1} \rangle_m + c\langle \mathcal{M}|\vec{v}|^2 D^{-1} \rangle_m \end{aligned} \tag{26}$$

For each of the conserved moments ($\mathcal{M} = 1$, v_x, v_y, $|\vec{v}|^2$) a new expression is found, allowing for the definition of a full rank system of linear equations:

$$\mathcal{A} \cdot G = \mathcal{B} \tag{27}$$

$$\mathcal{A} = \begin{bmatrix} \langle \frac{1}{D} \rangle_m & \langle \frac{v_x}{D} \rangle_m & \langle \frac{v_y}{D} \rangle_m & \langle \frac{|\vec{v}|^2}{D} \rangle_m \\ \cdot & \langle \frac{v_x^2}{D} \rangle_m & \langle \frac{v_x v_y}{D} \rangle_m & \langle \frac{v_x |\vec{v}|^2}{D} \rangle_m \\ \cdot & \cdot & \langle \frac{v_y^2}{D} \rangle_m & \langle \frac{v_y |\vec{v}|^2}{D} \rangle_m \\ \cdot & \cdot & \cdot & \langle \frac{|\vec{v}|^4}{D} \rangle_m \end{bmatrix} \tag{28}$$

$$G = \begin{bmatrix} a & b_x & b_y & c \end{bmatrix}^\top \tag{29}$$

$$\mathcal{B} = \begin{bmatrix} \rho & \rho u_x & \rho u_y & \rho |\vec{u}|^2/2 + \rho k T \end{bmatrix}^\top \tag{30}$$

where the matrix $\mathcal{A}$ is symmetric and redundant entries are not shown. Using the solution of this system of equations the thinker gas velocity distribution can be written as:

$$f_t = f_m(1 + \mathcal{D}) = f_m D^{-1} g = f_m D^{-1} (\mathcal{A}^{-1}\mathcal{B}) \cdot G \tag{31}$$

For arbitrary diameter functions, the terms in the matrix $\mathcal{A}$ and its inverse are most easily found by numerical methods. See the supplemental information for functional forms of $\mathcal{A}$ matrices for selected diameter functions.

Reinforcement learning implementation. Standard policy optimization algorithms [70, 77] were implemented to allow thinker learning during MD simulations. Particles were rewarded by their location within a simulated domain, effectively specifying a minimum-time locomotion task. Artificial feed-forward neural networks were used to encode two functions, the actor and critic. These functions are maps between a 'state' vector (in this case $\mathcal{S} = [x, y, v_x, v_y]$) and other quantities of interest. The critic maps states to expected future rewards (r):

$$\mathcal{C}(\mathcal{S}_t) \to \mathbb{E}\left[\int_\tau^\infty \gamma_r^{t-\tau} r_t dt\right] \tag{32}$$

where $\gamma_r < 1$ is the discount factor that bounds predictions to a finite time horizon. The actor simply maps states to actions ($P(\mathcal{S}_t) \to a_t$). The critic network is trained using the temporal difference (TD) target:

$$C(\mathcal{S}_t) \leftarrow C(\mathcal{S}_t) + \alpha(r_t + \gamma_r C(\mathcal{S}_{(t+\Delta t)}) - C(\mathcal{S}_t)) \tag{33}$$

where α is the learning rate and Δt is the time interval between updates. Note that we must wait until time $t + \Delta t$ to apply learning updates to functions evaluated at time t. The TD target is saved for use as an advantage estimator when training the actor network [78]. The actor function is updated in batches using the target:

$$P_\theta(\mathcal{S}_t) \leftarrow P_\theta(\mathcal{S}_t) + \alpha \nabla_\theta ln\ P_\theta(\mathcal{S}_t) A_t \tag{34}$$

where θ are the parameters of the network and A_t is the TD advantage estimator. To improve stability, the actor's evolution during a single update is clipped to a neighborhood in action probability space [70]. In these simulations, the thinker gas interacts with a bath of passive, fixed-diameter particles. At the shortest timescales ($t_{act} = 1$), the thinkers choose new diameters as a function of their experienced state $\mathcal{S}$ and actor network. At a longer timescale ($t_{learn} = 5$), the parameters of the actor and critic networks are updated. State transition tuples are accumulated in a memory buffer, and the critic and actor networks are trained by stochastic descent on these samples. All particles contribute experience to the same networks, and since the thinkers comprise only 10% of simulations, the effect is equivalent to parallel simulations of single thinkers in passive baths with pooled network parameters (centralized learning, decentralized actions). In all learning cases a simple feed-forward neural network architecture was used with 3 hidden layers of size 10. Neurons utilized the swish activation function [79].

A variety of simulation types were used as environments for learning. In the isothermal setting (Fig. 5c), a velocity Verlet integrator with Nosé-Hoover thermostat was used (temperature $k_b T = 1$) in a two-dimensional periodic simulation domain. In the vibrated granular bed model (Fig. 5d), a modified Langevin integrator was used in an xy-periodic simulation domain. Stochastic forces consistent with the fluctuation-dissipation relation ($\gamma = 0.1$, unity mean kinetic energy) were applied to particles, albeit with the z-component of these forces emphasized over in-plane components by a factor of 10. A floor was simulated as a frictionless plane (normal $\hat{n} = [0, 0, 1]$) that interacted via a potential with particles:

$$V_{wall}(r_n) = 4\varepsilon \left[\left(\frac{\sigma}{r_n}\right)^{12} - \left(\frac{\sigma}{r_n}\right)^{6}\right] + \varepsilon$$

for $r_n < r_{cut}$ and $V_{wall} = 0$ otherwise, where $\varepsilon = 1$, $\sigma = 1$, $r_{cut} = 2^{1/6}$, and r_n is the point-plane distance $r_n = \hat{n} \cdot \vec{x} + \vec{x_0}$ (plane normals are chosen so that r_n is always positive).

In the magnetic gas environment (Fig. 5e), isothermal conditions were applied to a 2D gas in a periodic domain. A Lorentz force with magnitude $B = 0.5$ was applied to induce curved particle trajectories. Finally, in the sheared gas environment (Fig. 5f) a body force $F_{y+} = (0.1, 0)$ was applied to particles with y-position greater than zero and $F_{y-} = (-0.1, 0)$ otherwise. Sheared particles evolved under standard (isotropic) Langevin integration ($\gamma = 0.1$, $k_b T = 1$) in a periodic 2D domain.

Simulations of odd gases utilized a transverse reciprocal force between particles of the form

$$F_{\mathrm{Lub}}(r) = \varepsilon \log\left(\frac{r_{cut}}{r - \Delta}\right) \tag{35}$$

for $r < (r_{cut} + \Delta)$ and $F_{Lub} = 0$ otherwise, where $\Delta = (D_i + D_j)/2$ and D_i, D_j are the diameters of

the interacting pair. Particles were integrated under Langevin dynamics, with damping parameter $\gamma = 0.1$. The strength of the transverse force was chosen to produce a gas with $k_bT_{eff} = 1$ in the steady state.

Pattern design in dropped and vibrated thinker grains. Simulations of thinker grains falling from a hopper and forming patterns were carried out using Langevin integration ($k_bT = 0$). Particles were released from a square aperture of size $10D_l$ at a height of $300/D_s$. Particles accelerated under a vertical force of strength 10γ, where $\gamma = 0.01$ is the Langevin damping parameter. Box walls, floor, and hopper surfaces were simulated as frictionless planes. Particles settled into a stationary layer on the floor of the chamber after a simulated time of $t_f = 1000$.

Vibrated pattern simulations were conducted as described for the vibrated granular bed model, with $\gamma = 0.01$, unity mean kinetic energy, and vertical stochastic forces 10 times as strong as those in-plane. To sequentially write out frames a new target configuration was set for thinkers and evolution was simulated for $t_p = 450$ time units. To prepare for the next frame, a 'clearing' run of duration $t_c = 150$ was performed during which red thinkers sought the box edge and cyan thinkers sought the box center. This clearing procedure assisted in distributing red thinkers equally over the domain and avoiding frame-to-frame correlations.

Thinker behavior rules were generated from an image of the desired character. The image was binarized, skeletonized, and converted to a set of points corresponding to bright pixels in the processed image. Thinkers decided their preferred diameter state by calculating the derivative of a field of Gaussian potentials ($\vec{\xi}$) emitted by these points (with width $\sigma = L_{box}/10\sqrt{2}$). For red thinkers, when $\vec{v}\cdot\vec{\xi} > 0$, the small diameter state was adopted, and the large diameter otherwise. The cyan thinker species had the same rule, but flipped the sign of calculated $\vec{\xi}$. The ability of thinkers to form and maintain patterns was principally a function of the ratio of their large and small diameter states. See the SI for images of patterned formed by other diameter ratios (section S7).

For comparison with worker particles, the same director field was used, however instead of feeding into eq. 8, a constant force of magnitude $F = D_s/\varepsilon = 1$ was applied to particles along it (for red particles), or antiparallel to it (for blue). Worker diameters were held constant at the average of thinker large and small diameters, $D_w = (D_s + D_l)/2$. All other simulation conditions were identical to the thinker comparison.

[1] Gašper Tkacik and William Bialek, "Information processing in living systems," The Annual Review of Condensed Matter Physics is **7**, 12–1 (2016).

[2] Ulrich Hopfer, "A maxwell's demon type of membrane transport: possibility for active transport by abc-type transporters?" Journal of theoretical biology **214**, 539–547 (2002).

[3] Sosuke Ito and Takahiro Sagawa, "Maxwell's demon in biochemical signal transduction with feedback loop," Nature communications **6**, 1–6 (2015).

[4] Yuhai Tu, "The nonequilibrium mechanism for ultrasensitivity in a biological switch: Sensing by maxwell's demons," Proceedings of the National Academy of Sciences **105**, 11737–11741 (2008).

[5] Pablo Sartori, Léo Granger, Chiu Fan Lee, and Jordan M Horowitz, "Thermodynamic costs of information processing in sensory adaptation," PLoS computational biology **10**, e1003974 (2014).

[6] Pablo Sartori and Simone Pigolotti, "Thermodynamics of error correction," Physical Review X **5**, 041039 (2015).

[7] David Andrieux and Pierre Gaspard, "Nonequilibrium generation of information in copolymerization processes," Proceedings of the National Academy of Sciences **105**, 9516–9521 (2008).

[8] David W Stephens and John R Krebs, "Foraging theory," in *Foraging theory* (Princeton university press, 2019).

[9] E. E. van Loon, J. Shamoun-Baranes, W. Bouten, and S. L. Davis, "Understanding soaring bird migration through interactions and decisions at the individual level," Journal of Theoretical Biology **270**, 112–126 (2011).

[10] Gottfried Sachs, "Minimum shear wind strength required for dynamic soaring of albatrosses," Ibis **147**, 1–10 (2005).

[11] Stefano Palagi and Peer Fischer, "Bioinspired microrobots," Nature Reviews Materials **3**, 113–124 (2018).

[12] Tian-Yun Huang, Hongri Gu, and Bradley J Nelson, "Increasingly intelligent micromachines," Annual Review of Control, Robotics, and Autonomous Systems **5**, 279–310 (2022).

[13] Marc Z Miskin, Alejandro J Cortese, Kyle Dorsey, Edward P Esposito, Michael F Reynolds, Qingkun Liu, Michael Cao, David A Muller, Paul L McEuen, and Itai Cohen, "Electronically integrated, mass-manufactured, microscopic robots," Nature **584**, 557–561 (2020).

[14] Michael F Reynolds, Alejandro J Cortese, Qingkun Liu, Zhangqi Zheng, Wei Wang, Samantha L Norris, Sunwoo Lee, Marc Z Miskin, Alyosha C Molnar, Itai Cohen, *et al.*, "Microscopic robots with onboard digital control," Science Robotics **7**, eabq2296 (2022).

[15] Harvey Leff and Andrew F Rex, *Maxwell's Demon 2 Entropy, Classical and Quantum Information, Computing* (CRC Press, 2002).

[16] L. Szilard, "On the decrease of entropy in a thermodynamic system by the intervention of intelligent beings," Zeitschrift für Physik **53**, 840–856 (1929).

[17] R. Landauer, "Irreversibility and Heat Generation in the Computing Process," IBM Journal of Research and Development **5**, 183–191 (1961), conference Name: IBM Journal of Research and Development.

[18] Charles H Bennett, "The thermodynamics of computation—a review," International Journal of Theoretical Physics **21**, 905–940 (1982).

[19] Martin B Plenio and Vincenzo Vitelli, "The physics of forgetting: Landauer's erasure principle and information theory," Contemporary Physics **42**, 25–60 (2001).

[20] Shoichi Toyabe, Takahiro Sagawa, Masahito Ueda, Eiro Muneyuki, and Masaki Sano, "Experimental demonstra-

tion of information-to-energy conversion and validation of the generalized jarzynski equality," Nature physics **6**, 988–992 (2010).
[21] Antoine Bérut, Artak Arakelyan, Artyom Petrosyan, Sergio Ciliberto, Raoul Dillenschneider, and Eric Lutz, "Experimental verification of landauer's principle linking information and thermodynamics," Nature **483**, 187–189 (2012).
[22] Averell L Gnatt, Patrick Cramer, Jianhua Fu, David A Bushnell, and Roger D Kornberg, "Structural basis of transcription: an rna polymerase ii elongation complex at 3.3 å resolution," Science **292**, 1876–1882 (2001).
[23] Charles S Peskin, Garrett M Odell, and George F Oster, "Cellular motions and thermal fluctuations: the brownian ratchet," Biophysical journal **65**, 316–324 (1993).
[24] H Wang and G Oster, "Ratchets, power strokes, and molecular motors," Applied Physics A **75**, 315–323 (2002).
[25] Elio A Abbondanzieri, William J Greenleaf, Joshua W Shaevitz, Robert Landick, and Steven M Block, "Direct observation of base-pair stepping by rna polymerase," Nature **438**, 460–465 (2005).
[26] Viviana Serreli, Chin-Fa Lee, Euan R Kay, and David A Leigh, "A molecular information ratchet," Nature **445**, 523–527 (2007).
[27] Joachim Frank and Ruben L Gonzalez Jr, "Structure and dynamics of a processive brownian motor: the translating ribosome," Annual review of biochemistry **79**, 381 (2010).
[28] Wonmuk Hwang and Martin Karplus, "Structural basis for power stroke vs. brownian ratchet mechanisms of motor proteins," Proceedings of the National Academy of Sciences **116**, 19777–19785 (2019).
[29] Roberto Di Leonardo, Luca Angelani, Dario Dell'Arciprete, Giancarlo Ruocco, Valerio Iebba, Serena Schippa, Maria Pia Conte, Francesco Mecarini, Francesco De Angelis, and Enzo Di Fabrizio, "Bacterial ratchet motors," Proceedings of the National Academy of Sciences **107**, 9541–9545 (2010).
[30] M Cristina Marchetti, Jean-François Joanny, Sriram Ramaswamy, Tanniemola B Liverpool, Jacques Prost, Madan Rao, and R Aditi Simha, "Hydrodynamics of soft active matter," Reviews of modern physics **85**, 1143 (2013).
[31] Pawel Romanczuk, Markus Bär, Werner Ebeling, Benjamin Lindner, and Lutz Schimansky-Geier, "Active brownian particles," The European Physical Journal Special Topics **202**, 1–162 (2012).
[32] Amin Doostmohammadi, Jordi Ignés-Mullol, Julia M Yeomans, and Francesc Sagués, "Active nematics," Nature communications **9**, 1–13 (2018).
[33] Lailai Zhu, Eric Lauga, and Luca Brandt, "Self-propulsion in viscoelastic fluids: Pushers vs. pullers," Physics of fluids **24**, 051902 (2012).
[34] Jeremie Palacci, Stefano Sacanna, Asher Preska Steinberg, David J. Pine, and Paul M. Chaikin, "Living Crystals of Light-Activated Colloidal Surfers," Science **339**, 936–940 (2013), publisher: American Association for the Advancement of Science.
[35] Clemens Bechinger, Roberto Di Leonardo, Hartmut Löwen, Charles Reichhardt, Giorgio Volpe, and Giovanni Volpe, "Active particles in complex and crowded environments," Reviews of Modern Physics **88**, 045006 (2016).
[36] J Tailleur and ME Cates, "Statistical mechanics of interacting run-and-tumble bacteria," Physical review letters **100**, 218103 (2008).
[37] Antoine Bricard, Jean-Baptiste Caussin, Debasish Das, Charles Savoie, Vijayakumar Chikkadi, Kyohei Shitara, Oleksandr Chepizhko, Fernando Peruani, David Saintillan, and Denis Bartolo, "Emergent vortices in populations of colloidal rollers," Nature communications **6**, 1–8 (2015).
[38] Julien Deseigne, Olivier Dauchot, and Hugues Chaté, "Collective motion of vibrated polar disks," Physical review letters **105**, 098001 (2010).
[39] Tzer Han Tan, Alexander Mietke, Junang Li, Yuchao Chen, Hugh Higinbotham, Peter J Foster, Shreyas Gokhale, Jörn Dunkel, and Nikta Fakhri, "Odd dynamics of living chiral crystals," Nature **607**, 287–293 (2022).
[40] Mark J Bowick, Nikta Fakhri, M Cristina Marchetti, and Sriram Ramaswamy, "Symmetry, thermodynamics, and topology in active matter," Physical Review X **12**, 010501 (2022).
[41] John Toner and Yuhai Tu, "Flocks, herds, and schools: A quantitative theory of flocking," Phys. Rev. E **58**, 4828–4858 (1998).
[42] Paul J. Flory and John Rehner, "Statistical mechanics of cross-linked polymer networks i. rubberlike elasticity," The Journal of Chemical Physics **11**, 512–520 (1943).
[43] Frank Jülicher, Armand Ajdari, and Jacques Prost, "Modeling molecular motors," Reviews of Modern Physics **69**, 1269 (1997).
[44] JMR Parrondo and B Jiménez de Cisneros, "Energetics of brownian motors: a review," Applied Physics A **75**, 179–191 (2002).
[45] Mónica Alvarez-Pérez, Stephen M Goldup, David A Leigh, and Alexandra MZ Slawin, "A chemically-driven molecular information ratchet," Journal of the American Chemical Society **130**, 1836–1838 (2008).
[46] Dibyendu Mandal and Christopher Jarzynski, "Work and information processing in a solvable model of maxwell's demon," Proceedings of the National Academy of Sciences **109**, 11641–11645 (2012).
[47] Jordan M Horowitz, Takahiro Sagawa, and Juan MR Parrondo, "Imitating chemical motors with optimal information motors," Physical review letters **111**, 010602 (2013).
[48] R Dean Astumian, "Kinetic asymmetry allows macromolecular catalysts to drive an information ratchet," Nature communications **10**, 1–14 (2019).
[49] John Bechhoefer, *Control Theory for Physicists* (Cambridge University Press, 2021).
[50] Joshua A Anderson, Jens Glaser, and Sharon C Glotzer, "Hoomd-blue: A python package for high-performance molecular dynamics and hard particle monte carlo simulations," Computational Materials Science **173**, 109363 (2020).
[51] John G Kirkwood, "Statistical mechanics of fluid mixtures," The Journal of chemical physics **3**, 300–313 (1935).
[52] Takahiro Sagawa and Masahito Ueda, "Second law of thermodynamics with discrete quantum feedback control," Physical review letters **100**, 080403 (2008).
[53] Francisco J Cao and M Feito, "Thermodynamics of feedback controlled systems," Physical Review E **79**, 041118 (2009).
[54] Takahiro Sagawa and Masahito Ueda, "Generalized jarzynski equality under nonequilibrium feedback control," Physical review letters **104**, 090602 (2010).

[55] Chen Huang, Mingnan Ding, and Xiangjun Xing, "Information swimmer: Self-propulsion without energy dissipation," Physical Review Research **2**, 043222 (2020).
[56] Thomas M Cover and Joy A. Thomas, *Elements of information theory* (Wiley-Interscience, 2006).
[57] Juan MR Parrondo, Jordan M Horowitz, and Takahiro Sagawa, "Thermodynamics of information," Nature physics **11**, 131–139 (2015).
[58] Sunghan Ro, Buming Guo, Aaron Shih, Trung V Phan, Robert H Austin, Dov Levine, Paul M Chaikin, and Stefano Martiniani, "Model-free measurement of local entropy production and extractable work in active matter," Physical Review Letters **129**, 220601 (2022).
[59] LR G Treloar, *The physics of rubber elasticity* (OUP Oxford, 1975).
[60] Mehran Kardar, *Statistical physics of particles* (Cambridge University Press, 2007).
[61] Nikolai V Brilliantov and Thorsten Pöschel, *Kinetic theory of granular gases* (Oxford University Press on Demand, 2004).
[62] Eric Bertin, Michel Droz, and Guillaume Grégoire, "Boltzmann and hydrodynamic description for self-propelled particles," Physical Review E **74**, 022101 (2006).
[63] L. Biferale, F. Bonaccorso, M. Buzzicotti, P. Clark Di Leoni, and K. Gustavsson, "Zermelo's problem: Optimal point-to-point navigation in 2D turbulent flows using reinforcement learning," Chaos: An Interdisciplinary Journal of Nonlinear Science **29**, 103138 (2019), publisher: American Institute of Physics.
[64] Gautam Reddy, Antonio Celani, Terrence J. Sejnowski, and Massimo Vergassola, "Learning to soar in turbulent environments," Proceedings of the National Academy of Sciences **113**, E4877–E4884 (2016), publisher: Proceedings of the National Academy of Sciences.
[65] Siddhartha Verma, Guido Novati, and Petros Koumoutsakos, "Efficient collective swimming by harnessing vortices through deep reinforcement learning," Proceedings of the National Academy of Sciences **115**, 5849–5854 (2018), publisher: Proceedings of the National Academy of Sciences.
[66] Simona Colabrese, Kristian Gustavsson, Antonio Celani, and Luca Biferale, "Flow Navigation by Smart Microswimmers via Reinforcement Learning," Physical Review Letters **118**, 158004 (2017), publisher: American Physical Society.
[67] Yuguang Yang, Michael A. Bevan, and Bo Li, "Efficient Navigation of Colloidal Robots in an Unknown Environment via Deep Reinforcement Learning," Advanced Intelligent Systems **2**, 1900106 (2020).
[68] S. Muiños-Landin, A. Fischer, V. Holubec, and F. Cichos, "Reinforcement learning with artificial microswimmers," Science Robotics **6**, eabd9285 (2021), publisher: American Association for the Advancement of Science.
[69] Martin J Falk, Vahid Alizadehyazdi, Heinrich Jaeger, and Arvind Murugan, "Learning to control active matter," Physical Review Research **3**, 033291 (2021).
[70] John Schulman, Filip Wolski, Prafulla Dhariwal, Alec Radford, and Oleg Klimov, "Proximal policy optimization algorithms," CoRR **abs/1707.06347** (2017), 1707.06347.
[71] Florian Lang, Gillian L Busch, Markus Ritter, Harald Volkl, Siegfried Waldegger, Erich Gulbins, and Dieter Haussinger, "Functional significance of cell volume regulatory mechanisms," Physiological reviews **78**, 247–306 (1998).
[72] Else K Hoffmann, Ian H Lambert, and Stine F Pedersen, "Physiology of cell volume regulation in vertebrates," Physiological reviews **89**, 193–277 (2009).
[73] Ming Guo, Adrian F Pegoraro, Angelo Mao, Enhua H Zhou, Praveen R Arany, Yulong Han, Dylan T Burnette, Mikkel H Jensen, Karen E Kasza, Jeffrey R Moore, *et al.*, "Cell volume change through water efflux impacts cell stiffness and stem cell fate," Proceedings of the National Academy of Sciences **114**, E8618–E8627 (2017).
[74] John D. Weeks, David Chandler, and Hans C. Andersen, "Role of Repulsive Forces in Determining the Equilibrium Structure of Simple Liquids," The Journal of Chemical Physics **54**, 5237–5247 (1971).
[75] C. Cercignani, R. Illner, and M. Pulvirenti, *The Mathematical Theory of Dilute Gases*, Applied Mathematical Sciences (Springer New York, 1994).
[76] Carlo Cercignani, "Are there more than five linearly-independent collision invariants for the boltzmann equation?" Journal of statistical physics **58**, 817–823 (1990).
[77] Richard S. Sutton and Andrew G. Barto, *Reinforcement Learing: An Introduction*, 2nd ed. (MIT Press, Cambridge, MA, 2018).
[78] John Schulman, Philipp Moritz, Sergey Levine, Michael Jordan, and Pieter Abbeel, "High-dimensional continuous control using generalized advantage estimation," arXiv preprint arXiv:1506.02438 (2015).
[79] Prajit Ramachandran, Barret Zoph, and Quoc V. Le, "Searching for activation functions," CoRR **abs/1710.05941** (2017), 1710.05941

ACKNOWLEDGEMENTS

V.V. acknowledges support from the Simons Foundation, the National Science Foundation under grant DMR-2118415 and the University of Chicago Materials Research Science and Engineering Center, which is funded by the National Science Foundation under Grant DMR-2011854. B.V.S. acknowledges support from a MRSEC-funded (DMR-2011854) Kadanoff-Rice fellowship. Research was sponsored by the Army Research Office and was accomplished under Cooperative Agreement Number W911NF-22-2-0109. The views and conclusions contained in this document are those of the authors and should not be interpreted as representing the official policies, either expressed or implied, of the Army Research Office or the U.S. Government. The U.S. Government is authorized to reproduce and distribute reprints for Government purposes notwithstanding any copyright notation herein. This work was completed in part with resources provided by the University of Chicago Research Computing Center. The authors would like to thank M. Fruchart, K. Husain, D. Martin and A. Murugan for helpful conversations.

AUTHOR CONTRIBUTIONS

B.V.S. and V.V. contributed to the design of the study and writing of the manuscript. B.V.S. performed the

numerical simulations and analytical calculations.

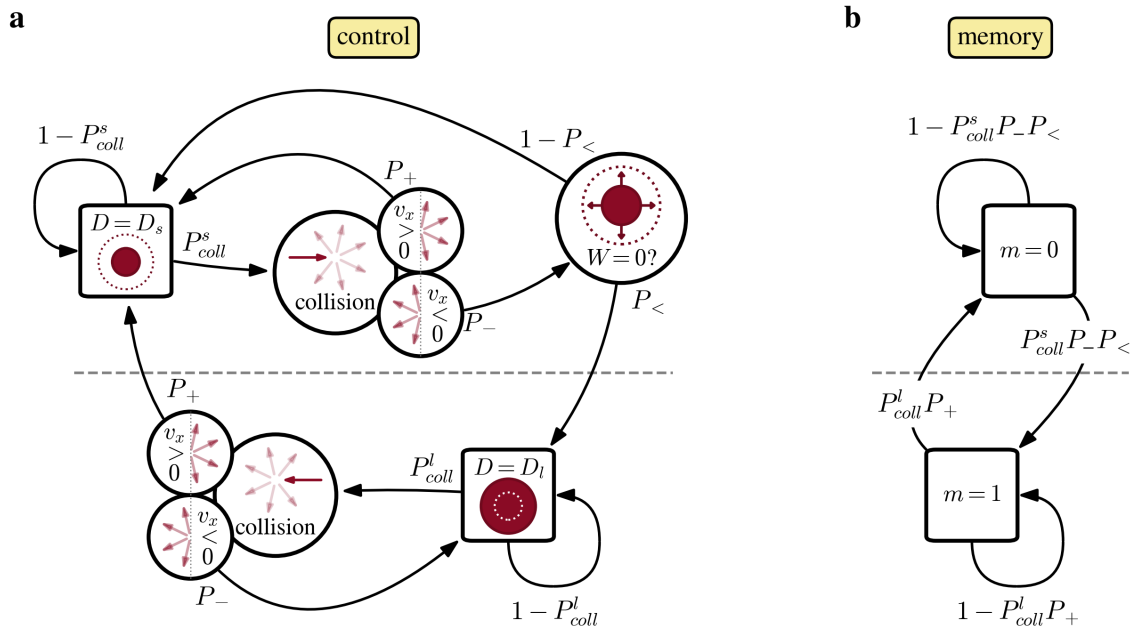

FIG. E1. **Markov chain model of the thinker measurement process**. **a** Transition diagram for thinkers with a diameter rule as in fig. 2**a**. Thinkers select one of two diameters depending on their current velocity. Collisions occur in the time between thinker actions (Δt) with probability P^l_{coll} (for large particles or P^s_{coll} for small) and randomize velocities (scattering into negative or positive velocities with probabilities P_- or P_+ respectively). For hard disks, shrinking diameter never requires the thinker to exert work on the surrounding gas ($W = 0$), but expansions are only possible if no other obstacles (i.e. particles) are nearby (probability $P_<$). **b** Condensed two-state Markov chain model transition diagram for the one-bit measurement that thinkers collect to determine which diameter state to adopt. In the steady state, the measurement sequence $M = [m_t, m_{t+\Delta t}, \dots]$ has a mean entropy per measurement, $H(M)$.

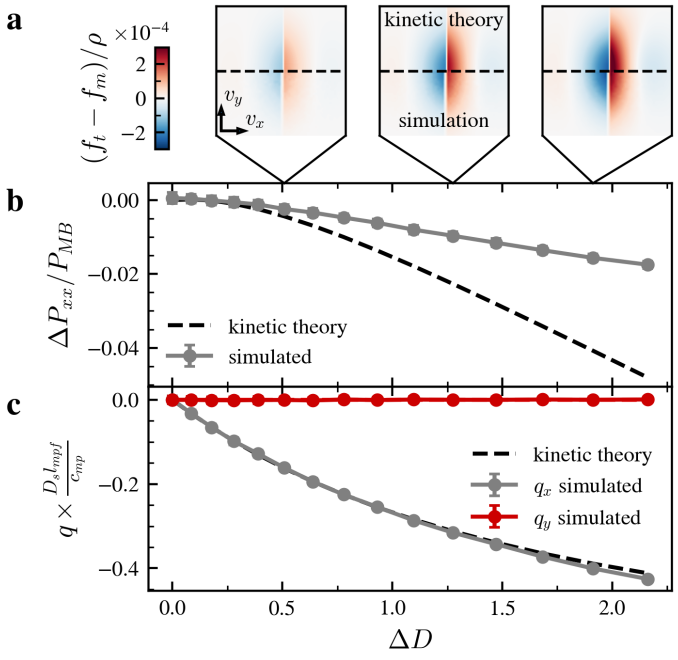

FIG. E2. **Comparison between kinetic theory of a pure thinker gas and a microscopic numerical model**. A pure gas of thinkers, following the simulation protocol and diameter rule of Fig. 2e-g and compared against theoretical predictions supplied by a kinetic theory. **a** Difference between the thinker velocity distribution function and the MB distribution, as obtained by kinetic theory and simulation. **b** Pressure in the x direction ($\Delta P_{xx}/P_{MB} = -\Delta P_{yy}/P_{MB}$). **c** Components of the heat flux vector, $\vec{q}$, normalized by the mean free path length l_{mfp} and most probable speed c_{mp}.

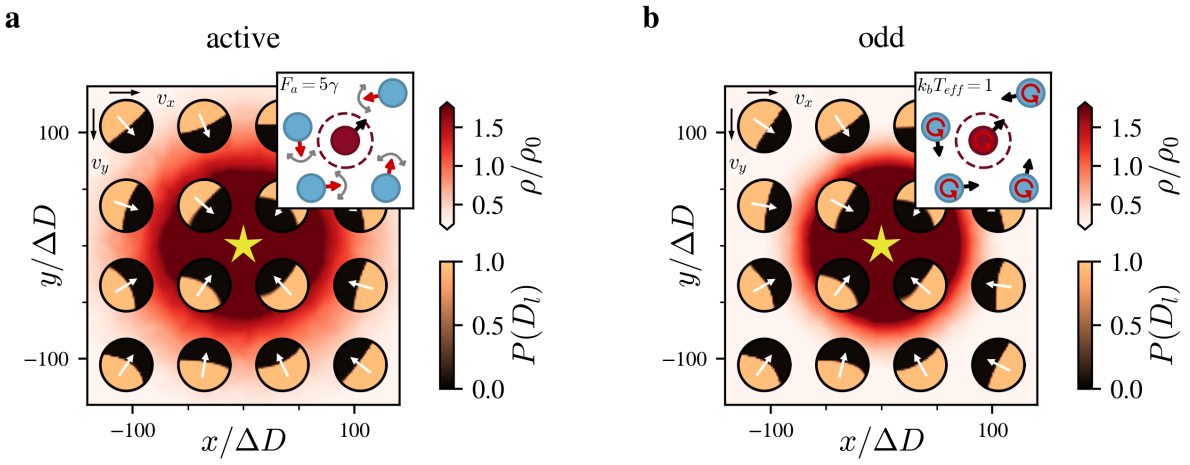

FIG. E3. **RL learning in active and odd gases**. Thinker gas agents immersed in an non-thermal gas. The learned solution is independent of the type of non-thermal agitation. **a** Thinkers learning a locomotion task (move to the location indicated by the star) within a gas of mechanically active particles. Mechanically active particles have a fixed-magnitude force $F_a = 5\gamma$ pointing along their director, where γ is the value of Langevin damping and the rotational diffusion constant of the active particles' directors. **b** Thinkers in an odd gas. All particles experience an equal and opposite transverse force during collisions, in addition to the usual hard core repulsion.

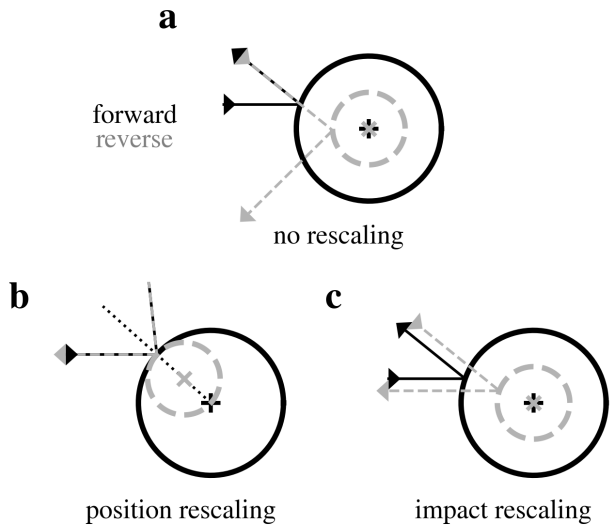

FIG. E4. **The microreversibility of hard disk collisions with velocity-dependent diameters.** Two particles of diameter $D(\vec{v}) = D$ and $D(\vec{v}_*) = D_*$ with velocities $\vec{v}$ and $\vec{v}_*$ are shown as the collision of a point object (with velocity $\vec{v}_* - \vec{v}$) with a stationary disk of diameter $D + D_*$. **a** In the coordinate frame centered on the stationary disk, the forward (black) and reverse (grey) collisions are not symmetric. **b** In the coordinate frame centered on the point of contact forward and reverse collision processes are symmetric, provided that the stationary disk's position is rescaled by a factor $(D' + D'_*)/(D + D_*)$ **c** The symmetry of the collision can also be preserved in the frame centered on the stationary disk by rescaling the impact parameter of the incoming particle.

Supplemental Information for "Informational active matter"

Bryan VanSaders[1] and Vincenzo Vitelli[1,2,3,*]

[1] *James Franck Institute, The University of Chicago, Chicago, Illinois 60637, USA*
[2] *Department of Physics, The University of Chicago, Chicago, Illinois 60637, USA*
[3] *Kadanoff Center for Theoretical Physics, The University of Chicago, Chicago, Illinois 60637, USA*

arXiv:2302.07402v1 [cond-mat.soft] 14 Feb 2023

Contents

S1. Defining informational activity 2
S1.1. The Maxwell demon 2
S1.2. Active Brownian particles 2
S1.3. Vicsek-like flockers 2
S1.4. RNA polymerase 3

S2. Energy conservation in Molecular Dynamics simulations of thinkers 3

S3. Thermodynamics of information for active matter 3
S3.1. Two state Markov chain model of an informational active process 5

S4. The thinker gas velocity distribution function 7
S4.1. Kinetic theory of hard disks 7
S4.2. Hard disk collisions with non-constant diameter 8
S4.3. The thinker gas collision invariant 9
S4.4. Demonstration of f_t as the steady-state solution to the variable-diameter collision operator 12
S4.5. Invertibility of the matrix $\mathcal{A}$ 13
S4.6. Diameter functions approaching zero 13

S5. Explicit form of $\mathcal{A}$ for select $D(\vec{v})$ 14
S5.1. Step function 14
S5.2. Anisotropic gaussian diameter function 16

S6. First order hydrodynamics of the thinker gas 17

S7. Pattern resolution in dropped thinker grains 20

S8. Description of Supplemental Videos 20
S8.1. Supplemental video S1 20
S8.2. Supplemental video S2 21

References 21

In §S1 the definition of informational activity is discussed along with several examples. In §S2 we demonstrate that the protocol used in Molecular Dynamics simulations of the thinker gas does not change the internal energy state of the system. Section §S3 describes how local measurements can drive non-equilibrium dynamics for a two-state Markov model. In §S4 a kinetic gas theory of the dilute pure thinker gas is developed in detail to accompany the abbreviated treatment in the main text methods. Section §S5 contains explicit functional forms for the moments of two thinker gases with special diameter functions. In §S6 the hydrodynamic consequences of the thinker kinetic gas theory are discussed. In §S7 compares pattern resolution for thinkers dropped from a hopper as a function of maximum thinker diameter. Finally, §S8 has descriptions of the two accompaning supplemental videos.

*Electronic address: vitelli@uchicago.edu

S1. DEFINING INFORMATIONAL ACTIVITY

We are concerned here with active media, many-body systems comprised of 'active' subunits. Multiple definitions of 'activity' can be found - here we will define an active subunit as one that has an internal process which biases its microstate transition probabilities (away from detailed balance, i.e. equilibrium). We focus on the distinction between two sub-classes of activity: 'mechanical' and 'informational' activity. Both varieties fulfil the transition biasing definition posed above, however their methods (and dependence on environmental noise) differ. Mechanical activity is familiar from many studies of self-propelled particles [1–13], and its key distinguishing feature is that subunits bias transitions by changing the free energy of the microstate *currently occupied* by the subunit. An iconic example is the active Janus particle, in which a local chemical reaction raises the free energy of the particle's current microstate in such a way that relaxation occurs by forward motion. Informational activity is the complementary strategy - biasing transitions by changing the free energy of *unoccupied* microstates which may become occupied in the future.

Many realistic active systems (particularly biological ones) will be driven by a mix of mechanical and informational activity. In order for informational activity to be possible, three key elements must be present:

1. **Noise**. Forces outside the subunit's control which act upon the d.o.f.s of interest are a requirement for informational activity. As only unoccupied microstates can be biased, informational activity does not directly drive transitions. Instead, some other source of agitation must be present.

2. **Ability to bias unoccupied microstates**. Microstates other than the one currently occupied by the subunit must be biased. Additionally, the applied bias must persist long enough for the subunit to interact with that microstate. Consider an unoccupied microstate, and a subunit about to transition into it. If a bias is applied, and immediately relaxes before the transition occurs, the bias has no effect and the microstate is now occupied.

3. **Measurement and feedback**. The capacity to measure the current microstate of the d.o.f.s of interest is central to informational activity. Unoccupied microstates can only be identified by determining the current subunit microstate. Furthermore, a feedback control loop must exist between the d.o.f.s of interest and the biasing of unoccupied states. If these two processes are decorrelated then biasing becomes merely another random process which is bound to obey detailed balance.

We now examine several key examples using these criteria.

S1.1. The Maxwell demon

In James Clerk Maxwell's iconic paradox [14], a 'demon' operates a trapdoor between two containers full of gas. By allowing only fast particles to cross from the left to right containers, and only slow to pass from right to left, a temperature gradient between the containers is produced. This happens despite the demon carefully opening or closing the trapdoor only when no gas particles are present at the junction between the containers. In this example, noise (in the form of a thermalized gas) plays a key role (requirement 1). The trapdoor fulfils requirement 2 - states where gas molecules occupy the doorway are not biased by closing the door. Rather, the door is closed preemptively to avoid an incoming particle crossing the wrong way. Feedback between the state of incoming gas particles and the state of the trapdoor fulfils requirement 3.

S1.2. Active Brownian particles

Active Brownian particles are self-propelled objects, usually smaller than a micron in size. In practice, they tend to operate by catalyzing a chemical reaction on half their surface, expansion of the reactants pushes them along. Such small objects exist at a scale where room temperature thermal fluctuations are important, satisfying requirement 1. However requirements 2 and 3 are not satisfied - particles have no capacity to measure their current microstate or modulate their chemically-derived force. Nor do they possess the capacity to bias unoccupied states (in the commonly considered overdamped regime).

S1.3. Vicsek-like flockers

The flocking of birds can be represented with a toy model of 'flying spins' in which particles have a polar variable, their heading, which interact similarly to magnetic dipoles [15]. Particles also typically have a fixed velocity magnitude

(imagined to be the result of self-propulsion) which points along their heading. Alignment interactions tend to draw nearby flockers into parallel trajectories. While flockers might be considered to 'measure' the heading of their neighbors, the resulting heading changes are deterministic processes, in which fluctuations play no role. When present, orientational noise is simply a disturbing influence that heading alignments fight against. Flocking models of this type are typically not informational because flockers drive transitions in their heading by forces acting directly on their current state. As such, their active properties are evident even in the absence of noise.

S1.4. RNA polymerase

The process of copying an RNA strand from template DNA is ubiquitous to cellular life, and is carried out by a complex molecular machine known as the RNA polymerase (RNAP). High fidelity [16] is important, as transcription errors could produce proteins that fail to fold, or are ineffective or harmful when folded. Like DNA polymerase, both selectivity and proofreading is employed to achieve high fidelity. Selectivity mechanisms are thought to closely resemble those employed by DNA [17, 18], while proofreading mechanisms are different. In RNAPs the active site where new nucleotides bind can be modulated. During elongation, this site facilitates the addition of incoming bases onto the growing RNA strand. For various reasons, RNAPs may undergo 'pausing' or 'backtracking', in which the progress of elongation is interrupted [19, 20]. Such events have been associated with expression regulation as well as error correction [21–23]. Single-molecule experiments on RNAPs have found evidence to support a 'Brownian ratchet' interpretation of the transcription process, whereby the polymerase moves down the template DNA stochastically and is rectified by the selectivity and proofreading processes [24].

The scale and stochastic behavior of RNAPs fulfill requirement 1 (noisy operation). RNAPs can be interpreted as biasing unoccupied states - specifically the states corresponding to incorrect base additions, which fulfils requirement 2. The ability of RNA polymerase to proofread (and to be selective for the correct base) are a form of measurement, where the conformation of the protein is changed according to an assessment of the template DNA strand or correct/incorrect state of the most recently added RNA base. Selectivity is relative to the pattern of the template DNA, a feedback process, fulfiling requirement 3.

S2. ENERGY CONSERVATION IN MOLECULAR DYNAMICS SIMULATIONS OF THINKERS

The thinker gas diameter changing protocol described in the main text methods is designed to avoid changing the potential or kinetic energy of the system (i.e. exert no mechanical work). As proof of the energy-conserving nature of the thinker gas numerical implementation, a test simulation using a constant-energy ensemble was prepared and the total energy of the system was monitored, shown in fig. S1. The implemented thinker gas algorithm does not inject or remove energy from the system at a rate greater than numerical precision effects under standard fixed-diameter dynamics.

S3. THERMODYNAMICS OF INFORMATION FOR ACTIVE MATTER

To understand the origin of activity in informational systems like the thinker gas, we will begin from basics by first describing the origin of mechanical activity in thermodynamic language. Consider an isothermal system which has had its Helmholtz free energy raised by an amount ΔF (perhaps as the result of an external field applied by a 'controller'). The controller must exert

$$W_{cont}^{in} \geq \Delta F \tag{S1}$$

work to accomplish this change, with saturation of the bound only for reversible processes with no heat transfer. Now that the system is prepared in a high-energy state it can perform work on some external load as it relaxes. This work is similarly

$$\mathcal{W}_{sys}^{out} \geq -\Delta F. \tag{S2}$$

where the sign of $\mathcal{W}_{sys}^{out}$ is negative. The controller exerts work W_{cont}^{in} so as to prepare the system to perform work $-\mathcal{W}_{sys}^{out} \leq W_{cont}^{in}$ on a load. Now consider replacing the controller with an active agent immersed in the system. If $\mathcal{W}_{sys}^{out}$ is used to move the active agent, then the above logic is unchanged except that the fate of $\mathcal{W}_{sys}^{out}$ is to be enventually converted completely to heat in dissipative processes.

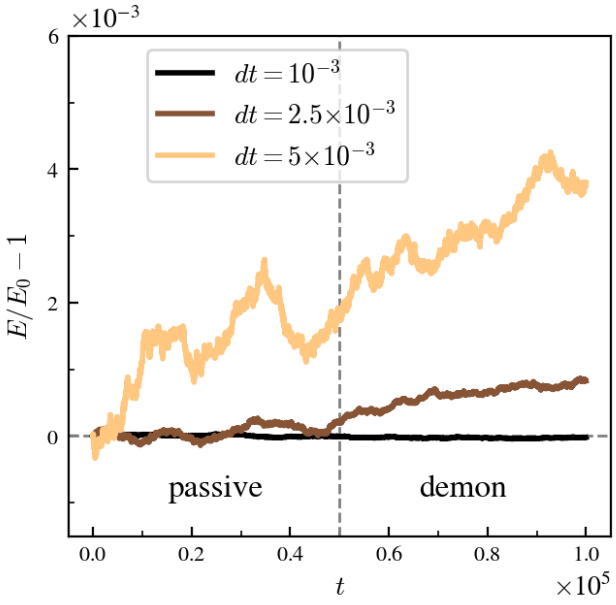

Fig. S1: **Total kinetic and potential energy of a numerically simulated thinker gas for various values of the time step parameter** dt**.** For times less than 5×10^4, the system is evolved under fixed-diameter dynamics with a constant-energy integrator. For $t > 5 \times 10^4$, diameter resizing is enabled. The diameter resizing procedure does not produce a detectable signature in the total energy drift of the system, which is controlled by the choice of dt.

When the active agent has the ability to collect measurements, equation S1 must be ammended with another term accounting for how information changes the entropy of the system [25],

$$W^{in}_{cont} + k_b T I \geq \Delta F. \tag{S3}$$

Where I is the mutual information of a measurement outcome and the microstate of the system. Even in the absence of work exerted by the agent, free energy differences in the system can be created (and therefore used to exert work on loads). Just as in the previous case, $\mathcal{W}^{out}_{sys} \geq -\Delta F$, yielding

$$\mathcal{W}^{out}_{sys} \geq -W^{in}_{cont} - k_b T I = -W^{in}_{cont} + T\Delta S \tag{S4}$$

where $\Delta S = -k_b I$ is the amount that the system's entropy has been reduced by the measurement. The work available to propel the active agent may be non-zero even for agents what exert no forces on the system that surrounds them.

When the action of an informational active agent is repeated (e.g. at intervals Δt), an additional complication arises where each new measurement outcome may be correlated with prior measurements. This dependence can be expressed as [26]:

$$\Delta S_t = -k_b \sum_t I(X_t; m_t | M_{0 \to t-\Delta t}) \tag{S5}$$

where X_t is the microstate measured at time t, m_t is the collected measurement, and $M_{0 \to t-\Delta t}$ is the history of measurements collected at prior times. The gained information is conditional on prior measurement outcomes - entropy is only lowered if a new measurement collects novel information about the system. When the measurements are error-free (i.e. they perfectly report the relevant microscopic information), eq. S5 can be expressed using the Shannon entropy of the measurement sequence:

$$\Delta S_t = -k_b H(M_{0 \to t}) \tag{S6}$$

where the Shannon entropy takes its usual form:

$$H(\mathcal{X}) = -\sum_{x\in\mathcal{X}} P(x)\ ln\ P(x) \tag{S7}$$

The entropy of the measurement history $M_{0\to t}$ is potentially complex to calculate for non-ergodic measurement ensembles. However our focus is on steady states of large collections of informational agents, so we will construct ergodic measurement ensembles with well-defined steady states. In this case the rate of entropy decrease per measurement by agent can be expressed as a limit:

$$\lim_{t\to\infty} \frac{\Delta S_t}{t} = \Delta\bar{S}. \tag{S8}$$

If the system can be represented as a steady Markov process, eq. S5 can be expressed as an entropy rate given by the weighted Shannon entropy of the relevant stochastic matrix:

$$\Delta\bar{S} = -k_b\bar{H}(M) = k_b\sum_{ij}\mu_i P_{ij}\ ln\ P_{ij} \tag{S9}$$

where $\mathbf{P}$ is the stochastic matrix that describes transitions between states [27] and μ is the accompanying stationary distribution.

To organize the distinction between mechanical and informational driving, it is useful to consider a mixed active process with a bound on the work it can exert on the system ($W < \epsilon$). Each time the active process acts, it takes a measurement to check if the action can be taken without violating the bound ϵ. Note that in cases where the mechanical work is capped at some value W_{max} (e.g. the maximum possible output torque of a motor), the bound only becomes relevant if $\epsilon < W_{max}$. Similarly, taking actions may require mechanical work (such as overcoming friction in a mechanism) that has no dependence on the particle or system's state. This kind of work is assumed to be small, or equivalently that the total bound includes an external and internal component, $\epsilon_{total} = \epsilon + \epsilon_{int}$. The 'internal' work bound covers the cost of internal inefficiencies of the active process, such as friction. Here we only consider variations of the 'external' work bound, which constrains the work done by the active process on the particle's, or system's, state. A particle with such a mixed process can be driven at most by

$$\bar{\mathcal{W}} \geq -\langle W\rangle_{(<\epsilon)} + k_bT\Delta\bar{S} \tag{S10}$$

where $\langle W\rangle_{(<\epsilon)}$ is the expected amount of mechanical work per action from actions that obey the bound ϵ. The mechanical contribution is not directly scaled by temperature, whereas the informational part grows (entropy changes due to measurement are always negative) with temperature, indicating that informational active agents grow stronger as fluctuations increase. This dependence on temperature is reminiscent of entropic elasticity [28–31], in which rubber-like materials grow stiffer as temperature is increased. To gain further insight into the work and entropy terms that make up eq. S10, we will now construct a Markov chain model of an active process with two discrete states.

S3.1. Two state Markov chain model of an informational active process

Consider a binary active processes, i.e. one that has only two states. This process is part of a measurement and feedback loop - the active process measures the system and determines if a change of state is warranted. We can describe this situation by focusing on the results of the measurement, the answer to the question "which state should I adopt?". This measurement m is binary valued ($m = 0$ or $m = 1$), and the answer fluctuates due to the noisy system. Measured values of $m = \{0, 1\}$ correspond to control actions, $c = \{0, 1\}$ - e.g. when a measurement $m = 0$ is collected, the control action $c = 0$ is performed on the system. Therefore, measured answers must respect the bound imposed by ϵ. If we represent the dynamics of the measurement variable m with a Markov chain, and focus on the long time limit in which a stationary distribution μ has been reached, we can compute the entropy rate directly using eq. S9. Let us start by specifying a simple but generic form of the transition matrix $\mathbf{P}$,

$$\mathbf{P} = \begin{bmatrix} 1-\alpha\Sigma & \alpha\Sigma \\ \beta\Sigma & 1-\beta\Sigma \end{bmatrix} \tag{S11}$$

where $\alpha\Sigma$ is the probability of the measured variable changing from $m_t = 0$ to $m_{t+\Delta t} = 1$, and $\beta\Sigma$ is the probability of the reverse transition of $m_t = 1$ to $m_{t+\Delta t} = 0$. The terms β and α represent the transition outcomes of some

stochastic process in the surrounding system, while Σ is the likelihood that taking the control action associated with measurement m will respect the work bound ϵ. Said another way, the controller would implement the control action $c = 1$ at a time $t + \Delta t$, given a prior state $m = 0$ at time t, with probability α. However the bound ϵ only permits this with probability Σ. For the transition matrix defined in eq. S11, the stationary distribution is

$$\mu = \left[\frac{\beta}{\beta+\alpha} \quad \frac{\alpha}{\beta+\alpha} \right], \tag{S12}$$

in which Σ has dropped out due to its symmetry.

Take as an instructive example the case of $\alpha = 1/2$, $\beta = 1/2$, $\Sigma = 1$. These parameters describe a delta-correlated random process (coin flips), in which the work bound never restricts the controller, and the entropy rate of this process reduces to $ln\ 2$. Generally, when $\alpha, \beta \neq 1/2$ longer-time correlations exist in the measurement stream - the value of m_{t+dt} becomes conditional on m_t. As we saw before in eq. S5, this reduces the amount of new information in each measurement.

We can gain further understanding by choosing a form for the probability of an action respecting the work bound, Σ. Consider a process where switching from control action $c = 0$ to $c = 1$ (or vice versa) dissipates an amount of work, with a probability distribution given by

$$P(W) = (1 - P_0)\frac{1}{\sigma}\sqrt{\frac{2}{\pi}}e^{-\frac{|W|^2}{\sigma^2}} + P_0\delta(0), \tag{S13}$$

where σ parameterizes the fluctuations of the system that affect expended work, δ is the impulse function ($\int \delta = 1$) and P_0 is the probability that the action costs zero work. The likelihood of this work falling below the bound set by ϵ is the integral:

$$\Sigma = \int_0^\epsilon P(W)dW = (1 - P_0)\ erf\left(\frac{\epsilon}{\sigma}\right) + P_0 \tag{S14}$$

where $erf()$ is the standard error function. We can also now write down the form of the mechanical work term in eq. S10:

$$\langle W \rangle_{(<\epsilon)} = \int_0^\epsilon W(P(W) - P_0\delta(0))dW = \frac{(1 - P_0)\sigma}{\sqrt{2\pi}}\left(1 - e^{-\frac{\epsilon^2}{\sigma^2}}\right) \tag{S15}$$

and so obtain a full expression for the bound of work done by the system per action on the active agent:

$$\bar{\mathcal{W}} \geq -\frac{(1 - P_0)\sigma}{\sqrt{2\pi}}\left(1 - e^{-\frac{\epsilon^2}{\sigma^2}}\right) + k_bT\bar{H}(M). \tag{S16}$$

For $\alpha = \beta = 1/2$, the terms of this equation are plotted in fig. S2 as a function of the ratio of the mechanical work bound to the work fluctuations (ϵ/σ). Note that σ can be a function of the temperature of the system, as well as other parameters of interaction. Consider a case where actions are prohibited by obstacles in the environment - σ will depend upon the fluctuations of those obstacles (i.e. k_bT) as well as parameters such as their mass or mechanical stiffness.

We see that the entropy-like contribution to the non-equilibrium free energy as $\epsilon \to 0$ is:

$$-k_bT\bar{H}(P_0\alpha) = k_bT\left(P_0\alpha\ ln\ P_0\alpha + (1 - P_0\alpha)\ ln\ (1 - P_0\alpha)\right), \tag{S17}$$

which is an entropy associated with the probability that actions will require zero work. Conversely, as $\epsilon \to 0$ the contribution from mechanical work approaches zero. In the limit of large ϵ, the informational contribution approaches $-k_bT\alpha = k_bT\ ln\ 2$, losing any dependence on the statistics of the constraint. The mechanical contribution approaches a value set by the details of σ. In the example shown here, $\sigma = 1$, however arbitrarily large values are possible. Despite this, the mechanical contribution will always equal zero as $\epsilon \to 0$

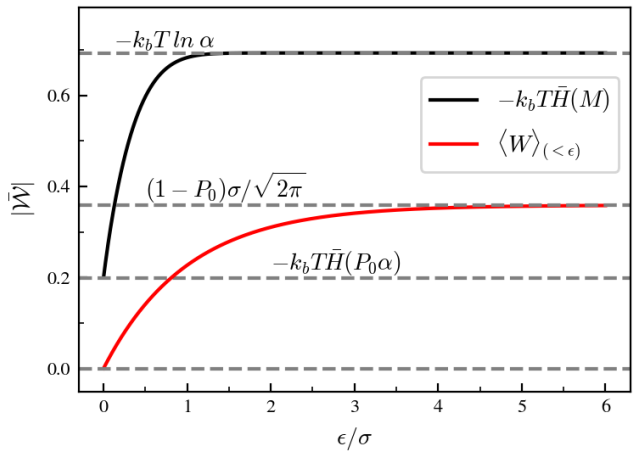

Fig. S2: **Propulsive power bounds for a mixed informational-mechanical Markov process**. A binary variable, updated by a simple Markov process that includes the effect of a mechanical work constraint, ϵ. Here σ is a variance associated with mechanical work exerted by the process, and P_0 is the likelihood of an action requiring no work. The transition probabilities are kept fixed at $\alpha = \beta = 1/2$. The total available power has an informational (black) and mechanical (red) contribution. In the limit of large ϵ/σ the informational process approaches the entropy of unconstrained transitions, and the mechanical work approaches a value controlled by the variation in how much mechanical work actions require (σ). Note that at finite ϵ the mechanical contribution may far exceed the informational contribution depending on the details of σ, however as $\epsilon \to 0$ the mechanical contribution always approaches zero. In contrast, informational driving only approaches zero as $\epsilon \to 0$ if $P_0 = 0$.

S4. THE THINKER GAS VELOCITY DISTRIBUTION FUNCTION

In order to derive an approximate description of the thinker gas velocity distribution function, we will outline key points from the derivation of the Boltzmann equation which describes the evolution of the same distribution for a hard sphere gas. More information on the derivation of the standard Boltzmann equation and its mathematical properties can be found in texts by Cercignani et al [32] and Kardar [33]. From there, the treatment is extended to the case of hard disks with non-constant diameters (which are functions of particle velocity only). We show the form of the collision operator which describes the thinker gas, and demonstrate that this operator has a modified collision invariant expression which includes the diameter function $D(\vec{v})$. We use this property to define a linear system of integral equations which permits solving for the deviation of the thinker gas velocity distribution function from the equilibrium Maxwell-Boltzmann (MB) distribution.

S4.1. Kinetic theory of hard disks

The evolution of a gas in phase space under the influence of interparticle collisions can be described by the BBGKY hierarchy. In this set of coupled differential equations the evolution of N-particle distribution functions (denoted $P^{(N)}$) are dependent upon the dynamics of $N+1$-particle distributions. The full hierarchy is in general too complex for useful prediction, and so it is often truncated to only include one and two-particle distributions. The single-particle distribution function ($P^{(1)}$) is obtained from the full system distribution function of N particles by marginalization:

$$P^{(1)}(\vec{x}_1, \vec{v}_1, t) = \int_{\mathcal{R}^{2N-2}} P(\vec{x}_1, \vec{v}_1, \vec{x}_2, \vec{v}_2, ..., \vec{x}_N, \vec{v}_N, t) d\vec{x}_1 d\vec{v}_1, ... d\vec{x}_N d\vec{v}_N \tag{S18}$$

This is the probability of finding a particle within the interval $[\vec{x}_1 + d\vec{x}, \vec{v}_1 + d\vec{v}_1, t + dt]$. The evolution of $P^{(1)}$ in the absence of collisions proceeds only by the streaming of particles along straight trajectories ($\partial P^{(1)}/\partial t = -\vec{v} \cdot \nabla_{\vec{x}} P^{(1)}$). Collisions between particles introduce a new operator to the equation of motion of the single-particle distribution:

$$\frac{\partial P^{(1)}}{\partial t} + \vec{v} \cdot \nabla_{\vec{x}} P^{(1)} = \mathcal{Q} \tag{S19}$$

$\mathcal{Q}$ describes the rate of change of particle number (or density) within the interval $[\vec{x} + d\vec{x}, \vec{v} + d\vec{v}, t + dt]$ caused by collisions. For hard spheres, collisions occur only when two particles are found in contact. Naturally, $\mathcal{Q}$ must

involve the two particle distribution, $P^{(2)}$ (the probability of finding two particles in a given configuration). If we denote pre-collision velocities for a pair of particles as $\vec{v}$ and $\vec{v}_*$, and their post-collision velocities as $\vec{v}'$ and $\vec{v}'_*$, we can write the collision operator as the difference of two rates, the gain and loss of particles within the interval of interest ($\mathcal{Q} = \mathcal{Q}^+ - \mathcal{Q}^-$). Particles are removed from the interval by collisions (velocities are transformed from $\vec{v}, \vec{v}_*$ to $\vec{v}', \vec{v}'_*$). The likelihood of a collision is the same as the likelihood of finding a two-particle configuration in contact. For particles of fixed diameter (D_0):

$$\mathcal{Q}^- = \frac{1}{2}\int_{\mathcal{R}^2}\int_{\mathcal{S}} P^{(2)}(\vec{x}, \vec{v}, \vec{x} + D_0\hat{n}, \vec{v}_*, t) d\vec{v}_* d\hat{n} \tag{S20}$$

here the variable $\hat{n}$ is a unit vector that lies along the particle contact vector and integration over $d\hat{n}$ occurs on the surface $\mathcal{S}$ of all possible contacts. For a gas in a periodic domain (homogeneous spatial density) the spatial aspect of $P^{(2)}$ can be approximated geometrically. A rectangular area with length $|(\vec{v}_* - \vec{v}) \cdot \hat{n}|dt$ and width $|D_0 d\hat{n}| = D_0$ contains the particles with velocity $\vec{v}_*$ which are capable of striking the first particle. The probability density of finding two particles with velocities $\vec{v}, \vec{v}_*$ in contact can therefore be written as:

$$\mathcal{Q}^- = \frac{1}{2}\int_{\mathcal{R}^2}\int_{\mathcal{S}^-} P^{(2)}(\vec{v}, \vec{v}_*, t)|(\vec{v}_* - \vec{v}) \cdot \hat{n}| D_0 d\vec{v}_* d\hat{n} \tag{S21}$$

where now location variables in $P^{(2)}$ have been dropped due to the assumption of spatial homogeneity. The inner integration is carried out over half the unit disk ($\mathcal{S}^-$, the half for which velocities $\vec{v}$ and $\vec{v}_*$ are approaching each other). This loss term is balanced (at steady state) by a similar term describing the gain of probability density by scattering from other regions of velocity space. The only differences being that the domain $\mathcal{S}^-$ is replaced by $\mathcal{S}^+$, the complementary hemisphere, and the velocities in consideration are $\vec{v}', \vec{v}'_*$, velocities which will undergo a scattering into $\vec{v}, \vec{v}_*$. As in the standard treatment, we will use the 'molecular chaos' assumption to replace two particle distribution terms with the product of single particle terms $P^{(2)}(\vec{v}, \vec{v}_*, t) \approx P^{(1)}(\vec{v}, t)P^{(1)}(\vec{v}_*, t)$. In the standard Boltzmann equation, the gain and loss terms are collected together under common integration limits by exploiting the time reversal symmetry of the collision process. Since we will now expand our treatment to include gases with diameters which are not constant in velocity space, we must examine the reversibility of hard disk collisions more closely.

S4.2. Hard disk collisions with non-constant diameter

We can find the velocities after collision between a pair of hard disks by conservation of momentum and energy. Assuming uniform particle masses, momentum and kinetic energy are conserved through the collision process:

$$\vec{v} + \vec{v}_* = \vec{v}' + \vec{v}'_* \tag{S22}$$

$$|\vec{v}|^2 + |\vec{v}_*|^2 = |\vec{v}'|^2 + |\vec{v}'_*|^2 \tag{S23}$$

This collision process can be viewed as the exchange of velocities projected onto the vector which points from one disk's center to the other. If $\hat{n}$ is a unit vector that points between disk centers at collision contact, then the post-collision velocities can be written as (for disks of equal mass):

$$\vec{v}' = \vec{v} - ((\vec{v} - \vec{v}_*) \cdot \hat{n})\hat{n} \tag{S24}$$

$$\vec{v}'_* = \vec{v}_* + ((\vec{v} - \vec{v}_*) \cdot \hat{n})\hat{n} \tag{S25}$$

For disks of fixed diameter, this scattering process is microreversible; $(\vec{v}, \vec{v}_*)$ map to $(\vec{v}', \vec{v}'_*)$ and $(-\vec{v}', -\vec{v}'_*)$ map to $(-\vec{v}, -\vec{v}_*)$, resulting in a Jacobian for the change of variables equal to -1 [32]. This one-to-one mapping allows all four velocity terms to be collected under the same unit disk integration in the standard Boltzmann collision operator.

When particle diameters are instead permitted to be functions of velocity, the microreversibility of the collision process is broken. We can see this diagrammatically in Fig. S3a. In this representation, we view the two particle collision process as the scattering of a point object with velocity $\vec{v}_* - \vec{v}$ off of a stationary disk with diameter $(D(\vec{v}) + D(\vec{v}_*))/2$. By changing the location of the stationary disk, the mapping of velocities can be preserved (fig. S3b). In a coordinate frame centered on the point of contact, the forward and reverse scattering process are symmetric provided that the coordinates of the stationary particle are scaled by a factor $(D(\vec{v}') + D(\vec{v}'_*))/(D(\vec{v}) + D(\vec{v}_*))$. The collision process can also be represented with the so-called 'impact parameter' (σ) as the integration variable (as opposed to the vector $\hat{n}$). Fig. S3c shows that a rescaling of the impact parameter has an equivalent effect of

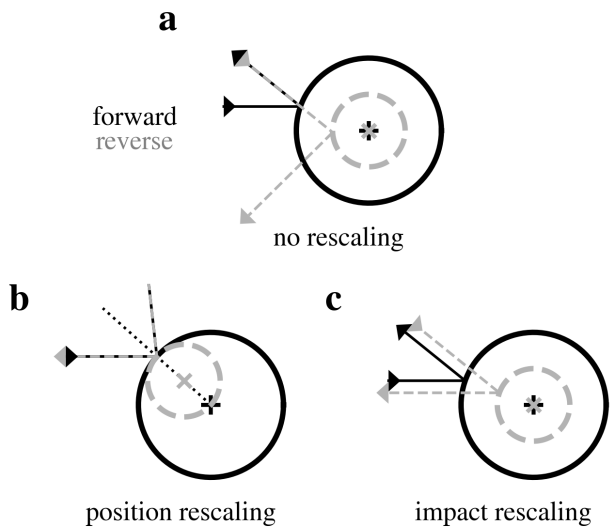

Fig. S3: **The microreversibility of hard disk collisions with velocity-dependent diameters.** Two particles of diameter $D(\vec{v}) = D$ and $D(\vec{v}_*) = D_*$ with velocities $\vec{v}$ and $\vec{v}_*$ are shown as the collision of a point object (with velocity $\vec{v}_* - \vec{v}$) with a stationary disk of diameter $D + D_*$. **a** In the coordinate frame centered on the stationary disk, the forward (black) and reverse (grey) collisions are not symmetric. **b** In the coordinate frame centered on the point of contact forward and reverse collision processes are symmetric, provided that the stationary disk's position is rescaled by a factor $(D' + D'_*)/(D + D_*)$ **c** The symmetry of the collision can also be preserved in the frame centered on the stationary disk by rescaling the impact parameter of the incoming particle.

preserving the velocity mapping. Naturally, the choice of rescaling one particle's position or the other is arbitrary and should produce equivalent results.

This mapping defines the procedure for exchanging unprimed and primed velocity variables in the collision operator of the thinker gas. From now on, we will refer to the single particle velocity distribution function as $f(\vec{x}, \vec{v}, t)$, and suppress the location and time arguments as we are concerned with the homogeneous steady-state solution. For brevity, functions of velocity will have their argument suppressed but retain distinguishing marks (such as $f(\vec{v}'_*) = f'_*$ and $D(\vec{v}'_*) = D'_*$). In this notation, we write the loss term of the thinker gas collision operator as:

$$\mathcal{Q}^- = \frac{1}{2}\int_{\mathcal{R}^2}\int_{\mathcal{S}^-}(D + D_*)ff_*|(\vec{v}_* - \vec{v})\cdot\hat{n}|d\vec{v}_*d\hat{n} \tag{S26}$$

The gain term can be expressed by the exchange of unprimed velocities for primed ones. The term $\vec{v}_* - \vec{v} = \vec{v}'_* - \vec{v}'$ is conserved by the collision process, and so need not be transformed.

$$\mathcal{Q}^+ = \frac{1}{2}\int_{\mathcal{R}^2}\int_{\mathcal{S}^+}(D' + D'_*)f'f'_*|(\vec{v}_* - \vec{v})\cdot\hat{n}|d\vec{v}'_*d\hat{n} \tag{S27}$$

These terms can be collected under a common integration, as the diameter function scaling acts a Jacobian term. The form of $\mathcal{Q}$ shown in the text is achieved by redistribution of diameter terms:

$$\mathcal{Q} = \mathcal{Q}^+ - \mathcal{Q}^- = \frac{1}{2}\int_{\mathcal{R}^2}\int_{\mathcal{S}}(D + D_*)|(\vec{v}_* - \vec{v})\cdot\hat{n}|\left[\frac{D' + D'_*}{D + D_*}f'f'_* - ff_*\right]d\vec{v}_*d\hat{n} \tag{S28}$$

Notice that the resulting collision operator is the sum of two terms that differ only by D and D_*. We will next consider the invariants of the thinker gas collision operator.

S4.3. The thinker gas collision invariant

We will first discuss collision invariants for the standard Boltzmann equation, and then explore the consequences of our modified thinker gas collision operator. If we consider a moment of a distribution function $f(\vec{v}, t)$ which is a solution to the Boltzmann equation with a non-time-varying test function ϕ:

$$\langle\phi\rangle_f = \int_{\mathcal{R}^d} f(\vec{v},t)\phi(\vec{v})d\vec{v} \tag{S29}$$

the evolution of this quantity is:

$$\frac{d}{dt}\langle\phi\rangle_f = \int_{\mathcal{R}^2} \phi(\vec{v})\mathcal{Q}(f)(\vec{v},t)d\vec{v} \tag{S30}$$

The function ϕ can be brought into the integrand of the collision operator since it is not a function of time. As we are now considering an expression integrating over all $\vec{v}$ and $\vec{v}_*$ (and by extension $\vec{v}'$ and $\vec{v}'_*$), the choice of primed and starred variables is entirely arbitrary. A standard procedure is to average over the exchange of velocity variables [32]. We first express the right side of eq. S30 (with $\mathcal{Q}$ appropriate for constant disks, and dropping velocity arguments where obvious) as:

$$\frac{1}{2}\int_{\mathcal{R}^2}\int_{\mathcal{R}^2}\int_{\mathcal{S}} \phi\left(f'f'_* - ff_*\right)|(\vec{v}_* - \vec{v})\cdot\hat{n}|D_0 d\vec{v}_* d\vec{v} d\hat{n} \tag{S31}$$

The exchange of starred and unstarred variables results in no change to the expression, allowing the average over this exchange to be written as:

$$\frac{1}{4}\int_{\mathcal{R}^2}\int_{\mathcal{R}^2}\int_{\mathcal{S}} (\phi+\phi_*)\left(f'f'_* - ff_*\right)|(\vec{v}_* - \vec{v})\cdot\hat{n}|D_0 d\vec{v}_* d\vec{v} d\hat{n} \tag{S32}$$

Exchanging primed variables (which can be done because of the microreversibility of the constant-diameter collision process), results in a change of sign. Therefore the result of averaging over both exchanges is:

$$\frac{1}{8}\int_{\mathcal{R}^2}\int_{\mathcal{R}^2}\int_{\mathcal{S}} (\phi+\phi_*-\phi'-\phi'_*)\left(f'f'_* - ff_*\right)|(\vec{v}_* - \vec{v})\cdot\hat{n}|D_0 d\vec{v}_* d\vec{v} d\hat{n} \tag{S33}$$

If ϕ is a quantity which is conserved through the collision, then $\frac{d}{dt}\langle\phi\rangle_f = 0$. This defines a summational collisional invariant for the system. For the Boltzmann equation, summational invariants can only be linear combinations of the microscopically conserved quantities, $\mathcal{M} = 1$, $\vec{v}$, $|\vec{v}|^2$, which are unchanged during collision by construction [34]. Therefore there exist constants $(a,\vec{b},c) \in \mathcal{R}\times\mathcal{R}^2\times\mathcal{R}$ such that:

$$\mathcal{M}(\vec{v}) = a + \vec{b}\cdot\vec{v} + c|\vec{v}|^2 \tag{S34}$$

The preceding discussion has been for the standard Boltzmann collision operator. We can follow the same logic for the thinker gas collision operator described in eq. S28. If we temporarily shorthand the gain term in the collision operator as $G = (f'f'_*)(D'+D'_*)/(D+D_*)$ and the loss term as $L = (ff_*)$, the result of averaging over primed and unprimed variables for the thinker gas can be written as:

$$\frac{1}{8}\int_{\mathcal{R}^2}\int_{\mathcal{R}^2}\int_{\mathcal{S}} (\phi(D+D_*)+\phi_*(D+D_*)-\phi'(D'+D'_*)-\phi'_*(D'+D'_*))\,(G-L)\,|(\vec{v}_* - \vec{v})\cdot\hat{n}|d\vec{v}_* d\vec{v} d\hat{n} \tag{S35}$$

where the leading term involving the function ϕ can be written as:

$$\phi(D+D_*)+\phi_*(D+D_*)-\phi'(D'+D'_*)-\phi'_*(D'+D'_*) = (\phi D+\phi_* D_*-\phi' D'-\phi'_* D'_*)+(\phi D_*+\phi_* D-\phi' D'_*-\phi'_* D'). \tag{S36}$$

If the entirety of eq. S36 is zero at all points in the velocity plane, then the quantity ϕ is stationary on the thinker distribution. The second term on the r.h.s. of eq. S36 contains only cross terms between starred and unstarred variables, and so all terms within it will integrate to the same value and the total term reduces to zero. An expression for the time evolution of a test function ϕ for the thinker gas can therefore be written with only the first term in the r.h.s. of eq. S36 as:

$$\frac{d}{dt}\langle\phi\rangle_{f_t} = -\frac{1}{2}\int_{\mathcal{R}^2}\int_{\mathcal{R}^2}\int_{\mathcal{S}} D\phi\left(f'f'_*\frac{D'+D'_*}{D+D_*} - ff_*\right)|(\vec{v}_*-\vec{v})\cdot\hat{n}|d\vec{v}_*d\vec{v}d\hat{n} \tag{S37}$$

From this representation, we can define a new test function, $g = D(\vec{v})\phi$. In order for the function ϕ to be stationary under the action of the thinker collision operator, the quantity g must be a collisional invariant (unlike the case for fixed-diameter disks, where ϕ itself must be invariant). For a collisionally invariant g there must exist constants which express it as a linear combination of microscopically conserved quantities: $g = a + \vec{b}\cdot\vec{v} + c|\vec{v}|^2 = D\mathcal{M}$. Note that an invariant test function for the MB distribution does not generically produce an invariant g for the thinker collision operator, due to the diameter rescaling. We will use this relation to define the velocity distribution function of the thinker gas. Beginning with the MB velocity distribution function in 2D:

$$f_m(\vec{v}) = \frac{m\rho}{2\pi kT}e^{-\frac{m|\vec{p}|^2}{2kT}} \tag{S38}$$

where $\vec{p} = \vec{v} - \langle\vec{v}\rangle = \vec{v} - \vec{u}$ is the velocity of the gas in the flow frame. We express the thinker gas distribution function as $f_t = (1+\mathcal{D})f_m$, where $\mathcal{D}$ is a function of velocity only. Since we seek the steady-state form of $\mathcal{D}$, we can treat $(1+\mathcal{D})$ as a non-time-varying test function operating on the MB distribution. We are searching for the form of this test function that has stationary expectation values on the MB velocity distribution under the action of the thinker gas collision operator. By substituting $\langle(1+\mathcal{D})\rangle_{f_m,\,\mathcal{Q}_d}$ for $\langle\phi\rangle_f$ in eq. S37, we see that steady state will be reached when $D(1+\mathcal{D})$ is a summational collision invariant. Finding the form of $\mathcal{D}$ amounts to specifying the four constants a, b_x, b_y, c which define the linear mixing of microscopically conserved quantities. These constants can be found if we require that the first four moments of the thinker gas velocity distribution are equal to the first four moments of the equilibrium MB distribution.

This requirement reflects the fact that thinker gas collisions microscopically conserve number, momentum, and kinetic energy, just as elastic collisions between fixed diameter disks. This requires that any re-sizing of the disks occurs between collisions. From a theoretical point of view, the gas is sparse enough to ignore the cases in which a diameter change post-collision must be delayed until the disks have sufficiently separated. This limitation on the ability of the disks to change their size is likely the most significant contributor to deviations from the theory at high densities or large maximum diameters.

The requirement that the first four moments of the thinker gas distribution are equal to those of the MB and can be written as:

$$\begin{aligned}\int_{\mathcal{R}^2}\mathcal{M}f_m d\vec{v} &= \int_{\mathcal{R}^2}\mathcal{M}(1+\mathcal{D})f_m d\vec{v}\\ 0 &= \int_{\mathcal{R}^2}\mathcal{M}\mathcal{D}f_m d\vec{v}\end{aligned} \tag{S39}$$

which highlights that the expectation value of the deviation of the thinker distribution ($\mathcal{D}$) must be zero for the first four moments. Note that this restriction does not constrain the third-order moments which define the heat flux tensor, or even the individual entries of the pressure tensor (derived from second-order moments). Only the trace of the pressure tensor is fixed relative to the MB distribution.

Using the expression for the thinker gas collision invariant, $g = D(1+\mathcal{D})$, we can trivially reorder to obtain $(1+\mathcal{D}) = gD^{-1}$. As a scalar function which must be greater than zero, division by D presents no problems. In practice, D need not even be non-zero everywhere, but instead only where the probability density of f_m is not infinitesimal. Using this expression for the thinker perturbation, and the notation for expectation value $\langle\phi\rangle_m = \int\phi f_m d\vec{v}$, we can write:

$$\begin{aligned}\langle\mathcal{M}\rangle_m &= \langle\mathcal{M}(1+\mathcal{D})\rangle_m\\ &= \langle\mathcal{M}gD^{-1}\rangle_m\\ &= a\langle\mathcal{M}D^{-1}\rangle_m + b_x\langle\mathcal{M}v_xD^{-1}\rangle_m + b_y\langle\mathcal{M}v_yD^{-1}\rangle_m + c\langle\mathcal{M}|\vec{v}|^2D^{-1}\rangle_m\end{aligned} \tag{S40}$$

For each of the conserved moments ($\mathcal{M} = 1,\ v_x,\ v_y,\ |\vec{v}|^2$) a new expression is found, allowing for the definition of a full rank system of linear equations:

$$\mathcal{A}\cdot G=\mathcal{B} \tag{S41}$$

$$\mathcal{A}=\begin{bmatrix} \langle\frac{1}{D}\rangle_m & \langle\frac{v_x}{D}\rangle_m & \langle\frac{v_y}{D}\rangle_m & \langle\frac{|\vec{v}|^2}{D}\rangle_m \\ \cdot & \langle\frac{v_x^2}{D}\rangle_m & \langle\frac{v_xv_y}{D}\rangle_m & \langle\frac{v_x|\vec{v}|^2}{D}\rangle_m \\ \cdot & \cdot & \langle\frac{v_y^2}{D}\rangle_m & \langle\frac{v_y|\vec{v}|^2}{D}\rangle_m \\ \cdot & \cdot & \cdot & \langle\frac{|\vec{v}|^4}{D}\rangle_m \end{bmatrix} \tag{S42}$$

$$G=\begin{bmatrix} a & b_x & b_y & c \end{bmatrix}^\top \tag{S43}$$

$$\mathcal{B}=\begin{bmatrix} \rho & \rho u_x & \rho u_y & \rho|\vec{u}|^2/2+\rho kT \end{bmatrix}^\top \tag{S44}$$

where $\mathcal{A}$ is symmetric and redundant entries are not shown. Using the solution of this system of equations the thinker gas velocity distribution can be written as:

$$f_t=f_m(1+\mathcal{D})=f_mD^{-1}g=f_mD^{-1}(\mathcal{A}^{-1}\mathcal{B})\cdot G \tag{S45}$$

S4.4. Demonstration of f_t as the steady-state solution to the variable-diameter collision operator

We can show directly that the above procedure for finding a thinker gas distribution function solves $\mathcal{Q}(f_t)=0$ by examining the collision operator written as:

$$\mathcal{Q}=\frac{1}{2}\int_{\mathcal{R}^2}\int_{\mathcal{S}}B(\vec{v}_*,\vec{v},\hat{n})\left[(D'+D'_*)f'f'_*-(D+D_*)ff_*\right]d\vec{v}_*d\hat{n} \tag{S46}$$

in which the cross-section terms have been redistributed and the kernel term has been collected into a function B for brevity. Focusing on the term in brackets (Q), we can replace f with $f_t=D(1+\mathcal{D})f_m$:

$$Q\equiv(D'+D'_*)(1+\mathcal{D}')f'_m(1+\mathcal{D}'_*)f'_{m*}-(D+D_*)(1+\mathcal{D})f_m(1+\mathcal{D}_*)f_{m*} \tag{S47}$$

First, note that the Maxwellian distribution is the exponential of a collision invariant, or:

$$ln\ f_m+ln\ f_{m*}-ln\ f'_m-ln\ f'_{m*}=0 \tag{S48}$$

$$\frac{f_mf_{m*}}{f'_mf'_{m*}}=1 \tag{S49}$$

Equation S49 allows for eq. S47 to be written as:

$$\begin{aligned} Q=\ & f_mf_{m*}\left[D'(1+\mathcal{D}')+\mathcal{D}'_*D'(1+\mathcal{D}')+D'_*(1+\mathcal{D}'_*)+\mathcal{D}'D'_*(1+\mathcal{D}'_*)\right] \\ & +f_mf_{m*}\left[D(1+\mathcal{D})-\mathcal{D}_*D(1+\mathcal{D})-\mathcal{D}_*(1+\mathcal{D}_*)-\mathcal{D}D_*(1+\mathcal{D}_*)\right] \end{aligned} \tag{S50}$$

Recall that the quantity $g=D(1+\mathcal{D})$ is also a collision invariant. We simplify eq. S50 to:

$$Q=f_mf_{m*}\left[g'+g'_*-g-g_*\right]+f_mf_{m*}\left[g'\mathcal{D}'_*+g'_*\mathcal{D}'-g\mathcal{D}_*-g_*\mathcal{D}\right] \tag{S51}$$

The first term in eq. S51 is zero, by the definition of collision invariants. The second term is also equal to zero, because each of the four terms individually integrate to zero. The logic for each term is identical, so we will focus on $f_mf_{m*}g\mathcal{D}_*$:

$$\begin{aligned} q(g,\mathcal{D}_*)\ &\equiv-\tfrac{1}{2}\textstyle\int_{\mathcal{R}^2}\int_{\mathcal{S}}B(\vec{v}_*,\vec{v},\hat{n})f_mf_{m*}g\mathcal{D}_*d\vec{v}_*d\hat{n} \\ &=-\tfrac{1}{2}gf_m\textstyle\int_{\mathcal{R}^2}\int_{\mathcal{S}}B(\vec{v}_*,\vec{v},\hat{n})\mathcal{D}_*f_{m*}d\vec{v}_*d\hat{n} \end{aligned} \tag{S52}$$

Recall that the collision kernel B for hard disk collisions is a linear function of relative velocity. Therefore, eq. S52 is a first-order moment of $\mathcal{D}f_m$, which must equal zero by construction (see eq. S39). The other terms in eq. S51 can all be likewise shown to equal zero by exchange of velocity variables and use of eq. S49.

S4.5. Invertibility of the matrix $\mathcal{A}$

$\mathcal{A}$ can be written as the element-wise expectation over $f_m D^{-1}$ of the symmetric matrix:

$$\mathbb{E}_{f_m D^{-1}} \begin{bmatrix} 1 & v_x & v_y & |\vec{v}|^2 \\ . & v_x^2 & v_x v_y & v_x|\vec{v}|^2 \\ . & . & v_y^2 & v_y|\vec{v}|^2 \\ . & . & . & |\vec{v}|^4 \end{bmatrix} \tag{S53}$$

This matrix can be written as the outer product of two vectors (therefore it has rank one):

$$\begin{bmatrix} 1 & v_x & v_y & |\vec{v}|^2 \end{bmatrix}^\top \begin{bmatrix} 1 & v_x & v_y & |\vec{v}|^2 \end{bmatrix} \tag{S54}$$

Despite this, $\mathcal{A}$ is generically invertible. The element-wise expectation promotes the matrix to full rank. If we temporarily adopt the notation of $\langle\phi\rangle = \int \phi D^{-1} f_m d\vec{v}$, $\mathcal{A}$ can be written as:

$$\begin{bmatrix} \langle 1\rangle & \langle v_x\rangle & \langle v_y\rangle & \langle|\vec{v}|^2\rangle \\ \langle v_x\rangle & \langle v_x^2\rangle & \langle v_x v_y\rangle & \langle v_x|\vec{v}|^2\rangle \\ \langle v_y\rangle & \langle v_x v_y\rangle & \langle v_y^2\rangle & \langle v_y|\vec{v}|^2\rangle \\ \langle|\vec{v}|^2\rangle & \langle v_x|\vec{v}|^2\rangle & \langle v_y|\vec{v}|^2\rangle & \langle|\vec{v}|^4\rangle \end{bmatrix} \tag{S55}$$

The determinant of this matrix can be found by cofactor expansion along the first column. If we examine the determinant of the first of the four 3×3 matrices which make up $\mathcal{A}$, we find that a term composed of the difference of permutations of expectation values is produced:

$$\langle 1\rangle \begin{vmatrix} \langle v_x^2\rangle & \langle v_x v_y\rangle & \langle v_x|\vec{v}|^2\rangle \\ \langle v_x v_y\rangle & \langle v_y^2\rangle & \langle v_y|\vec{v}|^2\rangle \\ \langle v_x|\vec{v}|^2\rangle & \langle v_y|\vec{v}|^2\rangle & \langle|\vec{v}|^4\rangle \end{vmatrix} \tag{S56}$$

$$= \langle 1\rangle \left(\langle v_x^2\rangle\langle v_y^2\rangle - \langle v_x v_y\rangle^2\right)\langle|\vec{v}|^4\rangle$$

$$+\langle 1\rangle \left(\langle v_x v_y\rangle\langle v_x\rangle\langle v_y\rangle + \langle v_x\rangle^2\langle v_y\rangle^2 - \langle v_x^2\rangle\langle v_y\rangle^2 - \langle v_x\rangle^2\langle v_y^2\rangle\right)\langle|\vec{v}|^2\rangle^2 \tag{S57}$$

which will be nonzero due to the non-independence of the terms being exchanged through the expectation operator. All four sub-matrices follow this same pattern, with no requirements on the form of D^{-1}. Provided that $D > 0$ across the velocity plane, A can be numerically inverted without difficulty.

S4.6. Diameter functions approaching zero

The expression for the thinker gas involves the term $1/D$, implying that particle diameters must always remain finite for reasonable solutions to exist. As a demonstration, we can construct a diameter function with a single minimum which is nonzero by a small value ε:

$$D(\vec{v}, \varepsilon) = 1 - e^{-(|\vec{v}|^2/v_{th})^2} + \varepsilon \tag{S58}$$

where v_{th} is the mean thermal speed of particles. In fig. S4 slices through the velocity distribution function for various values of ε are shown. As $\varepsilon \to 0$, a probability density spike develops. This can be understood physically by considering the rate of collision for particles near the minimum. Such particles have greatly reduced collision rates (and so change velocities very slowly) compared to particles at velocities with finite diameters. For a D with a true zero, particles would never leave the point of phase space where collisions could not occur. This region would behave as a particle sink, from which it would be impossible to scatter back out of. Accordingly, the distribution function would become a delta function and the distribution entropy would diverge. The approach to that divergence is shown by the cuts in fig. S4.

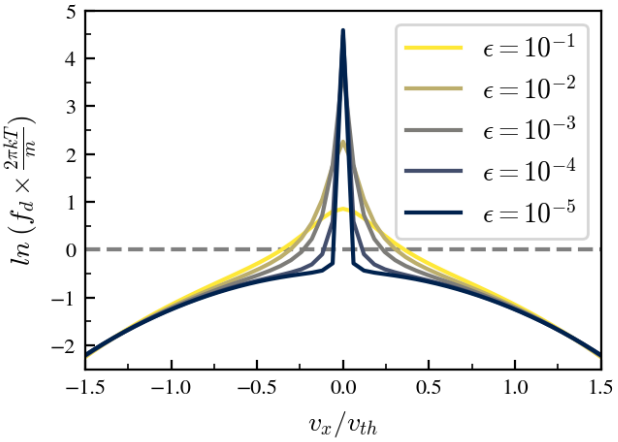

Fig. S4: **Velocity distribution function for thinker gases with a minima approaching zero.** A slice through $v_y = 0$ of the velocity distribution function (f_t) for a diameter function $D = 1 - e^{-|\vec{v}|^2/v_{th}^2} + \varepsilon$. As the minimum of D approaches zero, a density spike in velocity space develops.

S5. EXPLICIT FORM OF $\mathcal{A}$ FOR SELECT $D(\vec{v})$

The matrix $\mathcal{A}$ which defines the thinker gas velocity distribution function involves finding the expectation value (over the MB distribution) of several functions of velocity multiplied with the inverse diameter function (D). For arbitrary D these Gaussian integrals may become too cumbersome to find analytically, and numerical integration is expedient. In this appendix we will present explicit equations for the $\mathcal{A}$ matrices of two special D functions - a diameter step function, and an anisotropic Gaussian diameter function. These matrices may in principle be inverted analytically through a process such as finding the adjugate matrix. The equations for such a process rapidly become unwieldy however, so we will instead use a semi-analytical approach of finding $\mathcal{A}$ exactly, then performing a numerical inverse and estimating small-value derivatives of the relevant constants a, b_x, b_y, and c numerically. This numerical procedure can of course be extended to estimate the values of the $\mathcal{A}$ matrix for diameter functions which do not admit feasible analytic integration.

S5.1. Step function

A convenient diameter function can be written using the Heaviside step function:

$$D(\vec{v}) = D_s + (D_l - D_s)\mathbb{H}\left(-\frac{\vec{v}\cdot\vec{\xi}}{|\vec{v}|}\right) \tag{S59}$$

As we will require D^{-1} in many formulas, it is useful to express this also with the Heaviside function:

$$D^{-1}(\vec{v}) = \frac{1}{D_l} + \left(\frac{1}{D_s} - \frac{1}{D_l}\right)\mathbb{H}\left(-\frac{\vec{v}\cdot\vec{\xi}}{|\vec{v}|}\right) \tag{S60}$$

where D_s and D_l are the small and large diameters respectively, and $\vec{\xi}$ is the normal vector of the large/small decision boundary. We will only consider fixed $\vec{\xi} = \begin{bmatrix}1 & 0\end{bmatrix}$ here. The value of the Heaviside step function at zero will here be taken to be zero (as opposed to 1/2). With this choice of $\vec{\xi}$, integrals over the velocity plane can be split into an integral over the entire plane in addition to an integral over the half plane ($x > 0$). Using well-known expressions for Gaussian integrals of the form $\int x^n \mathcal{N}(x)$ [35], the following components of the $\mathcal{A}$ matrix can be found for a Maxwell-Boltzmann distribution in 2D with bulk velocity $\vec{u}$, thermal energy k_bT and gas density ρ. Where it appears, erf() refers to the standard error function.

$$\mathcal{A}_{11} = \int D^{-1} f_m = \frac{1}{D_l} + \frac{1}{2}\left(\frac{1}{D_s} - \frac{1}{D_l}\right)\left(1 - \mathrm{erf}\left(-u_x\sqrt{\frac{m}{2k_bT}}\right)\right) \tag{S61}$$

$$\mathcal{A}_{12} = \mathcal{A}_{21} = \int v_x D^{-1} f_m = \frac{1}{D_l}u_x + \left(\frac{1}{D_s} - \frac{1}{D_l}\right)\left(\frac{1}{2}u_x\left(\mathrm{erf}\left(-u_x\sqrt{\frac{m}{2k_bT}}\right) - 1\right) - \sqrt{\frac{k_bT}{2\pi m}}e^{-\frac{m}{2k_bT}u_x^2}\right) \tag{S62}$$

$$\mathcal{A}_{13} = \mathcal{A}_{31} = \int v_y D^{-1} f_m = \frac{1}{D_l}u_y + \left(\frac{1}{D_s} - \frac{1}{D_l}\right)\frac{1}{2}u_y\left(1 - \mathrm{erf}\left(-u_x\sqrt{\frac{m}{2k_bT}}\right)\right) \tag{S63}$$

$$\mathcal{A}_{14} = \mathcal{A}_{41} = \int |\vec{v}|^2 D^{-1} f_m = \int v_x^2 D^{-1} f_m + \int v_y^2 D^{-1} f_m = \mathcal{A}_{22} + \mathcal{A}_{33} \tag{S64}$$

$$\begin{aligned}\mathcal{A}_{22} = \int v_x^2 D^{-1} f_m = \quad & \frac{1}{D_l}\left(u_x^2 + \frac{k_bT}{m}\right) + \\ & \frac{1}{2}\left(\frac{1}{D_s} - \frac{1}{D_l}\right)\left(\left(u_x^2 + \frac{k_bT}{m}\right)\left(1 - \mathrm{erf}\left(-u_x\sqrt{\frac{m}{2k_bT}}\right)\right) + u_x\sqrt{\frac{k_bT}{2m\pi}}e^{-\frac{m}{2k_bT}u_x^2}\right)\end{aligned} \tag{S65}$$

$$\mathcal{A}_{33} = \int v_y^2 D^{-1} f_m = \frac{1}{D_l}\left(u_y^2 + \frac{k_bT}{m}\right) + \frac{1}{2}\left(\frac{1}{D_s} - \frac{1}{D_l}\right)\left(u_y^2 + \frac{k_bT}{m}\right)\left(1 - \mathrm{erf}\left(-u_x\sqrt{\frac{m}{2k_bT}}\right)\right) \tag{S66}$$

$$\begin{aligned}\mathcal{A}_{23} = \mathcal{A}_{32} = \int v_x v_y D^{-1} f_m = \quad & \frac{1}{D_l}u_x u_y + \\ & \left(\frac{1}{D_s} - \frac{1}{D_l}\right)\left(\frac{u_x u_y}{2}\left(1 - \mathrm{erf}\left(-u_x\sqrt{\frac{m}{2k_bT}}\right)\right) + u_y\sqrt{\frac{k_bT}{2\pi m}}e^{-\frac{m}{2k_bT}u_x^2}\right)\end{aligned} \tag{S67}$$

$$\mathcal{A}_{24} = \mathcal{A}_{42} = \int v_x|\vec{v}|^2 D^{-1} f_m = \int v_x^3 D^{-1} f_m + \int v_x v_y^2 D^{-1} f_m \tag{S68}$$

$$\begin{aligned}\int v_x^3 D^{-1} f_m = & \frac{1}{D_l}u_x\left(u_x^2 + \frac{3k_bT}{m}\right) + \\ & \left(\frac{1}{D_s} - \frac{1}{D_l}\right)\left(\frac{u_x}{2}\left(\left(u_x^2 + \frac{3k_bT}{m}\right)\left(1 - \mathrm{erf}\left(-u_x\sqrt{\frac{m}{2k_bT}}\right)\right) + \left(\frac{u_x^2}{2} + \frac{k_bT}{m}\right)\sqrt{\frac{2k_bT}{\pi m}}e^{-u_x^2\frac{m}{2k_bT}}\right)\right)\end{aligned}$$

$$\begin{aligned}\int v_x v_y^2 D^{-1} f_m = & \frac{1}{D_l}u_x\left(u_y^2 + \frac{k_bT}{m}\right) + \\ & \left(\frac{1}{D_s} - \frac{1}{D_l}\right)\left(u_y^2 + \frac{kT}{m}\right)\left(\frac{1}{2}u_x\left(1 - \mathrm{erf}\left(-u_x\sqrt{\frac{m}{2k_bT}}\right)\right) + \sqrt{\frac{k_bT}{2\pi m}}e^{-\frac{m}{2k_bT}u_x^2}\right)\end{aligned}$$

$$\mathcal{A}_{34} = \mathcal{A}_{43} = \int v_y|\vec{v}|^2 D^{-1} f_m = \int v_y v_x^2 D^{-1} f_m + \int v_y^3 D^{-1} f_m \tag{S69}$$

$$\begin{aligned}\int v_y v_x^2 D^{-1} f_m = & \frac{1}{D_l}u_y\left(u_x^2 + \frac{k_bT}{m}\right) + \\ & \left(\frac{1}{D_s} - \frac{1}{D_l}\right)\left[\frac{1}{2}u_y\sqrt{\frac{m}{2k_bT}}\left(u_x^2 + \frac{k_bT}{m}\right)\left(1 - \mathrm{erf}\left(-u_x\sqrt{\frac{m}{2k_bT}}\right)\right) + \frac{u_x u_y}{2\sqrt{\pi}}e^{-u_x^2\frac{m}{2k_bT}}\right]\end{aligned}$$

$$\int v_y^3 D^{-1} f_m = u_y\left(u_y^2 + \frac{3k_bT}{m}\right)\left[\frac{1}{D_l} + \frac{1}{2}\left(\frac{1}{D_s} - \frac{1}{D_l}\right)\left(1 - \mathrm{erf}\left(-u_x\sqrt{\frac{m}{2k_bT}}\right)\right)\right]$$

$$\mathcal{A}_{44} = \int |\vec{v}|^4 D^{-1} f_m = \int v_x^4 D^{-1} f_m + 2v_x^2 v_y^2 D^{-1} f_m + v_y^4 D^{-1} f_m \tag{S70}$$

$$\int v_x^4 D^{-1} f_m = \left(u_x^4 + \frac{6k_bT}{m}u_x^2 + \frac{3k_bT^2}{m^2}\right) \times \left[\frac{1}{D_l} + \frac{1}{2}\left(\frac{1}{D_s} - \frac{1}{D_l}\right)\left(1 - \mathrm{erf}\left(-u_x\sqrt{\frac{m}{2k_bT}}\right)\right)\right] + \left(\frac{1}{D_s} - \frac{1}{D_l}\right)\sqrt{\frac{k_bT}{2\pi m}}u_x e^{-u_x\sqrt{\frac{m}{2k_bT}}}\left(u_x^2 + 5\frac{k_bT}{m}\right)$$

$$\int 2v_x^2 v_y^2 D^{-1} f_m = \frac{2}{D_l}\left(u_x^2 + \frac{k_bT}{m}\right)\left(u_y^2 + \frac{k_bT}{m}\right) + \left(\frac{1}{D_s} - \frac{1}{D_l}\right)\left(u_y^2 + \frac{k_bT}{m}\right)\left[\left(u_x^2 + \frac{k_bT}{m}\right)\left(1 - \mathrm{erf}\left(-u_x\sqrt{\frac{m}{2k_bT}}\right)\right) + \sqrt{\frac{2k_bT}{\pi m}}u_x e^{-u_x^2\frac{m}{2k_bT}}\right]$$

$$\int v_y^4 D^{-1} f_m = \left(u_y^4 + \frac{6k_bT}{m}u_y^2 + \frac{3k_bT^2}{m^2}\right)\left[\frac{1}{D_l} + \left(\frac{1}{D_s} - \frac{1}{D_l}\right)\left(1 - \mathrm{erf}\left(-u_x\sqrt{\frac{m}{2k_bT}}\right)\right)\right]$$

S5.2. Anisotropic gaussian diameter function

Another form for D with comparatively simple integrals to compute is an anisotropic Gaussian:

$$D = e^{-\gamma_x\frac{m}{2k_bT}(v_x - u_x)^2} e^{-\gamma_y\frac{m}{2k_bT}(v_y - u_y)^2} \tag{S71}$$

where $\vec{u}$ is again the average velocity of the gas. The relative values of the constants γ_x and γ_x control the degree of anisotropy. This diameter function is particularly convenient because it can be merged with the MB distribution and integrated using the same functional forms:

$$\mathcal{A}_{11} = \int D^{-1} f_m = \frac{1}{\sqrt{1-\gamma_x}\sqrt{1-\gamma_y}} \tag{S72}$$

$$\mathcal{A}_{12} = \mathcal{A}_{21} = \int v_x D^{-1} f_m = \frac{u_x}{\sqrt{1-\gamma_y}\sqrt{1-\gamma_x}} \tag{S73}$$

$$\mathcal{A}_{13} = \mathcal{A}_{31} = \int v_x D^{-1} f_m = \frac{u_y}{\sqrt{1-\gamma_y}\sqrt{1-\gamma_x}} \tag{S74}$$

$$\mathcal{A}_{14} = \mathcal{A}_{41} = \mathcal{A}_{22} + \mathcal{A}_{33} \tag{S75}$$

$$\mathcal{A}_{22} = \int v_x^2 D^{-1} f_m = \frac{1}{\sqrt{1-\gamma_y}\sqrt{1-\gamma_x}}\left(u_x^2 + \frac{k_bT}{m}\frac{1}{(1-\gamma_x)}\right) \tag{S76}$$

$$\mathcal{A}_{33} = \int v_y^2 D^{-1} f_m = \frac{1}{\sqrt{1-\gamma_y}\sqrt{1-\gamma_x}}\left(u_y^2 + \frac{k_bT}{m}\frac{1}{(1-\gamma_y)}\right) \tag{S77}$$

$$\mathcal{A}_{23} = \mathcal{A}_{32} = \int v_x v_y D^{-1} f_m = \frac{u_x u_y}{\sqrt{1-\gamma_x}\sqrt{1-\gamma_y}} \tag{S78}$$

$$\mathcal{A}_{24} = \mathcal{A}_{42} = \int v_x |\vec{v}|^2 D^{-1} f_m = \int v_x^3 D^{-1} f_m + \int v_x v_y^2 D^{-1} f_m \tag{S79}$$

$$\int v_x^3 D^{-1} f_m = \frac{u_x}{\sqrt{1-\gamma_x}\sqrt{1-\gamma_y}}\left(u_x^2 + \frac{3k_bT}{m}\frac{1}{(1-\gamma_x)}\right)$$

$$\int v_x v_y^2 D^{-1} f_m = \frac{u_x}{\sqrt{1-\gamma_x}\sqrt{1-\gamma_y}}\left(u_y^2 + \frac{k_bT}{m}\frac{1}{(1-\gamma_y)}\right)$$

$$\mathcal{A}_{34} = \mathcal{A}_{43} = \int v_y |\vec{v}|^2 D^{-1} f_m = \int v_y v_x^2 D^{-1} f_m + \int v_y^3 D^{-1} f_m \tag{S80}$$

$$\int v_y^3 D^{-1} f_m = \frac{u_y}{\sqrt{1-\gamma_x}\sqrt{1-\gamma_y}} \left(u_y^2 + \frac{3k_bT}{m} \frac{1}{(1-\gamma_y)} \right)$$

$$\int v_y v_x^2 D^{-1} f_m = \frac{u_y}{\sqrt{1-\gamma_x}\sqrt{1-\gamma_y}} \left(u_x^2 + \frac{k_bT}{m} \frac{1}{(1-\gamma_x)} \right)$$

$$\mathcal{A}_{44} = \int v_x^4 D^{-1} f_m + 2 \int v_x^2 v_y^2 D^{-1} f_m + \int v_y^4 D^{-1} f_m \tag{S81}$$

$$\int v_x^4 D^{-1} f_m = \frac{1}{\sqrt{1-\gamma_x}\sqrt{1-\gamma_y}} \left(u_x^4 + u_x^2 \frac{6k_bT}{m} \frac{1}{(1-\gamma_x)} + 3 \left(\frac{k_bT}{m(1-\gamma_x)} \right)^2 \right)$$

$$\int 2v_x^2 v_y^2 D^{-1} f_m = \frac{2}{\sqrt{1-\gamma_x}\sqrt{1-\gamma_y}} \left(u_x^2 + \frac{k_bT}{m} \frac{1}{(1-\gamma_x)} \right) \left(u_y^2 + \frac{k_bT}{m} \frac{1}{(1-\gamma_y)} \right)$$

$$\int v_y^4 D^{-1} f_m = \frac{1}{\sqrt{1-\gamma_x}\sqrt{1-\gamma_y}} \left(u_y^4 + u_y^2 \frac{6k_bT}{m} \frac{1}{(1-\gamma_y)} + 3 \left(\frac{k_bT}{m(1-\gamma_y)} \right)^2 \right)$$

S6. FIRST ORDER HYDRODYNAMICS OF THE THINKER GAS

In this section we comment on the consequences of the thinker gas for first order hydrodynamics by examining the pressure tensor and heat flux. This procedure follows the standard treatment of a passive gas described by the Maxwell-Boltzmann distribution (see for instance, Kardar [33]), but instead utilizes the thinker gas distribution derived in section S4.

Quantities which are conserved microscopically relax at longer timescales than quantities which are not conserved in pair collisions these are denoted 'hydrodynamic' variables and are the main quantities to be described by a hydrodynamic theory. For elastic collisions particle number, components of linear momenta, and kinetic energy are conserved which result in hydrodynamic fields of density, flow velocity, and temperature. By definition, the thinker gas also conserves these quantities (however it has the freedom to redistribute conserved quantities over microscopic degrees of freedom). Regardless of the detailed form, the collision term in equation S30 can be replaced with the left-hand side of the Boltzmann equation, yielding the following expression for the evolution of a test function ϕ:

$$\frac{d}{dt}\langle\phi\rangle = \int_{\mathcal{R}^2} \phi \left[\partial_t + v_i \partial_i + \frac{F_i}{m} \frac{\partial}{\partial v_i} \right] f(\vec{x}, \vec{v}, t) = 0 \tag{S82}$$

where indices i are over Cartesian coordinates. This equation can be manipulated to yield an evolution equation for expectation values of the function ϕ:

$$\partial_t(\rho\langle\phi\rangle) + \partial_i(\rho\langle v_i\phi\rangle) - \rho\langle\partial_t\phi\rangle - \rho\langle v_i\partial_i\phi\rangle - \frac{\rho F_i}{m}\langle\partial\phi/\partial v_i\rangle = 0 \tag{S83}$$

Each of the conserved quantities can be evaluated with this expression to yield familiar hydrodynamic relations. First we define the local velocity, thermal velocity, pressure tensor, rate of strain tensor, and local kinetic energy and heat flux:

$$u_i = \langle v_i \rangle \tag{S84}$$

$$p_i = v_i - u_i \tag{S85}$$

$$P_{ij} = m\rho\langle p_i p_j \rangle \tag{S86}$$

$$u_{ij} = \frac{1}{2}(\partial_i u_i + \partial_j u_j) \tag{S87}$$

$$\epsilon = \langle \frac{1}{2} m |\vec{p}|^2 \rangle = \langle \frac{1}{2} m |\vec{v}|^2 - mv \cdot \vec{u} + \frac{1}{2} m |\vec{u}|^2 \rangle \tag{S88}$$

$$q = \frac{1}{2} m\rho\langle p_i |\vec{p}|^2 \rangle \tag{S89}$$

Hydrodynamic equations pertaining to the conservation of mass, momentum and energy read:

$$\partial_t \rho + \partial_i(\rho u_i) = 0 \tag{S90}$$

$$\partial_t u_i + u_j \partial_j u_i = \frac{F_i}{m} - \frac{1}{m\rho}\partial_j P_{ij} \tag{S91}$$

$$\partial_t \epsilon + u_i \partial_i \epsilon = -\frac{1}{\rho}\partial_i q_i - \frac{1}{\rho} P_{ij} u_{ij} \tag{S92}$$

In order to close this set of equations a form for the pressure tensor and heat flux is needed. These objects are found by taking expectation values of the single-particle probability distribution function, which is in general a function of space, velocity, and time. We will instead follow the standard approach of using a first order approximation of these quantities, found by taking modified expectation values over the homogeneous, steady-state distribution function derived in appendix S4. We begin in the usual way by noting that a mean free path timescale exists, which in the fixed-diameter case is approximately

$$\tau_\times \approx \frac{1}{\rho v_{th} D} \tag{S93}$$

where ρ is the number density of particles, v_{th} is a typical particle speed, and D is a fixed diameter. For the thinker gas, the above expression may be modified by considering that the mean diameter of the gas is the expectation of the diameter function over the velocity distribution:

$$\langle D \rangle_{f_t} = \int D f_t = \int D(1+\mathcal{D}) f_m \tag{S94}$$

For the purposes of this derivation, the mean diameter of the thinker gas will be considered to be fixed, and so $\tau_\times$ is taken to be the same in all directions. If we denote the previously discussed thinker gas velocity distribution for a homogeneous, steady-state gas as f_t^0, we now seek a first-order description of the deviations from this form (denoted f_t^1). We set $f_t^1 = f_t^0(1+h)$, where h describes this small deviation. Furthermore, we linearize the thinker collision operator as:

$$\mathcal{Q}_d^L[f_t^1] \approx -f_t^0 \frac{h}{\tau_\times} \tag{S95}$$

Using the following form of the Boltzmann equation which includes the effects of external forces ($\vec{F}$):

$$\frac{\partial f}{\partial t} + \vec{v} \cdot \nabla_{\vec{x}} f + \frac{\vec{F}}{m} \cdot \nabla_{\vec{v}} f = \mathcal{Q}(f) \tag{S96}$$

$$\mathcal{L}[f] = \mathcal{Q}(f) \tag{S97}$$

where $\mathcal{L}[f] = [\partial/\partial_t + v_i \partial/\partial_i + (F_i/m)\partial/\partial_{v_i}]\, f$ is a linear differential operator. Using the linearized collision operator approximation,

$$\mathcal{L}[f_t^1] \approx -f_t^0 \frac{h}{\tau_\times} \tag{S98}$$

$$h = -\tau_\times \frac{1}{f_t^0} \mathcal{L}[f_t^1] \approx -\tau_\times \mathcal{L}[ln\ f_t^0] \tag{S99}$$

where only the leading term as been retained. We now examine the term $\mathcal{L}[ln\ f_t^0]$:

$$ln\ f_t^0 = ln\ (f_m^0(1+\mathcal{D})) = ln\ (f_m^0 D^{-1} g) \tag{S100}$$

$$= ln\ f_m^0 - ln\ D + ln\ (a + \vec{b}\cdot\vec{v} + c|\vec{v}|^2) \tag{S101}$$

$$\mathcal{L}[ln\ f_t^0] = \mathcal{L}[ln\ f_m^0] - \mathcal{L}[ln\ D] + \mathcal{L}[ln\ (a + \vec{b}\cdot\vec{v} + c|v|^2)] \tag{S102}$$

We can express $h = h_m - h_D + h_g$ to emphasize that three terms contribute to the first order deviations. The first term, h_m, is unchanged from the standard first-order treatment of an equilibrium gas. Since we are only considering time-invariant diameter functions which are functions of velocity only, the second term will be equal to $-h_D = -(F_i/(mD))\partial D/\partial v_i$. Within the bulk of a gas with negligible body forces, this term will not contribute. The final term pertaining to the collision invariant g will have time and space derivatives arising from variations in the fields $T(\vec{x},t)$, $\vec{u}(\vec{x},t)$, and $\rho(\vec{x},t)$, as the values of $a, \vec{b}, c$ are constant for constant $T, \vec{u}, \rho$. We will denote such fields as Φ, and approximate the derivative of the constants $(\partial/\partial\Phi)[a, b_i, c] = [a^\Phi, b_i^\Phi, c^\Phi]$.

If we focus on a single term of the $\mathcal{L}$ operator, $v_i\partial/\partial_i$ (i.e. a steady-state, boundary-less system), and assume only a single field has spatial variation, we can illustrate the contributions from h_g.

$$v_i \frac{\partial ln\ g}{\partial x_i} = \frac{\partial g/\partial r_i}{g} \tag{S103}$$

$$= (a^\Phi + v_j b_j^\Phi + c^\Phi |\vec{v}|^2)\frac{1}{g}\frac{\partial \Phi}{\partial x_i} \tag{S104}$$

The expectation of first order-quantities like the pressure tensor and heat flux can be found by integration over the perturbed zeroth-order distribution:

$$\langle \mathcal{O} \rangle^1 = \int \mathcal{O} f_t^0 (1+h) = \langle \mathcal{O} \rangle^0 + \langle h\mathcal{O} \rangle^0 \tag{S105}$$

$$= \langle \mathcal{O} \rangle^0 + \langle h_m\mathcal{O} \rangle^0 - \langle h_D\mathcal{O} \rangle^0 + \langle h_g\mathcal{O} \rangle^0 \tag{S106}$$

For the pressure tensor ($\mathcal{O} = P_{ij}$) and the heat flux ($\mathcal{O} = q_i$), the contributions from the term $\langle h_m\mathcal{O}\rangle$ are unchanged from the standard treatment of a passive gas, resulting in heat flux terms which relax thermal gradients and off-diagonal pressure terms which relax shear flows. As noted above, the contributions from h_D will often be unimportant, so we focus on the term $\langle h_g\mathcal{O}\rangle$. The following forms of the pressure tensor and heat flux can be found:

$$P_{ij} = m\rho \sum_k \int f_m D^{-1} (a^\Phi + v_l b_l^\Phi + c^\Phi |\vec{v}|^2) \frac{\partial \Phi}{\partial x_k} v_k p_i p_j \tag{S107}$$

$$q_i = \frac{1}{2} m\rho \sum_k \int f_m D^{-1} (a^\Phi + v_l b_l^\Phi + c^\Phi |\vec{v}|^2) \frac{\partial \Phi}{\partial x_k} v_k p_i |\vec{p}|^2 \tag{S108}$$

Several remarks can be made about the first-order thinker corrections to P_{ij} and q_i, however first some comment about velocity reference frames must be made. The velocity, thermal velocity, and local velocity are related by $\vec{p} = \vec{v} - \vec{u}$. Kinetic theory is largely conducted in the $\vec{u}$ co-moving frame, which allows for the definition of familiar pressures, fluxes and temperatures. As the Maxwell-Boltzmann distribution is also defined in this frame, all is well. However for the thinker gas, we may define the particle's function of velocity in a global coordinate frame, or a local coordinate frame ($D(\vec{v})$ or $D(\vec{p})$). In this work we have chosen to use $D(\vec{v})$, except in the case of the anisotropic Gaussian function defined in appendix S5. This is because in any practical realization of a device like the thinkers described here, it is likely that knowledge of velocity in the global coordinate frame will be desirable or even required. In order for the operation of thinkers to induce fluxes towards a goal region, thinkers must be aware of the large-scale coordinate system which locates themselves and the target region. Furthermore, in such a case they are unconcerned with local fluxes relative to nearby flow, but rather absolute fluxes towards or away from the target.

Another consideration is the complexity of estimating the local average velocity of neighboring thinker particles. Simplistic methods of determining position (and hence velocity) such as utilizing a light gradient [36] inform particles of their coordinates in a global frame. Using similar methods to determine relative velocities to neighbors also raises a question of length scale - over what distance, practically, should particles consider their 'local' velocity neighborhood to extend?

Finally, the removal of a global coordinate frame for thinker particles would necessitate each particle to have an orientation vector. As this study concerns isotropic particles, particle orientations will not evolve during simulations unless an orientation-coupling force is defined, in a manner analogous to the Toner-Tu model of flocking [15]. For isotropic thinkers, such a choice would be arbitrary.

The mixed velocity components in eqs. S107 and S108 reflect the different considerations inherent to the operation of thinkers and the definition of the hydrodynamic equations of motion. First let us consider the case of $|\vec{u}| = 0$, in which $\vec{p} = \vec{v}$. In that case, the pressure tensor contains only one even moment of velocity and the term $f_m D^{-1}$. If D and f_m have inversion symmetry about the same point, then only the even term $(\sum_k \int f_m D^{-1} v_l v_k v_i v_j b_l^\Phi \partial\Phi/\partial x_i)$ will contribute to the pressure tensor corrections. However in the case of inversion-symmetric D, the constants b_i are

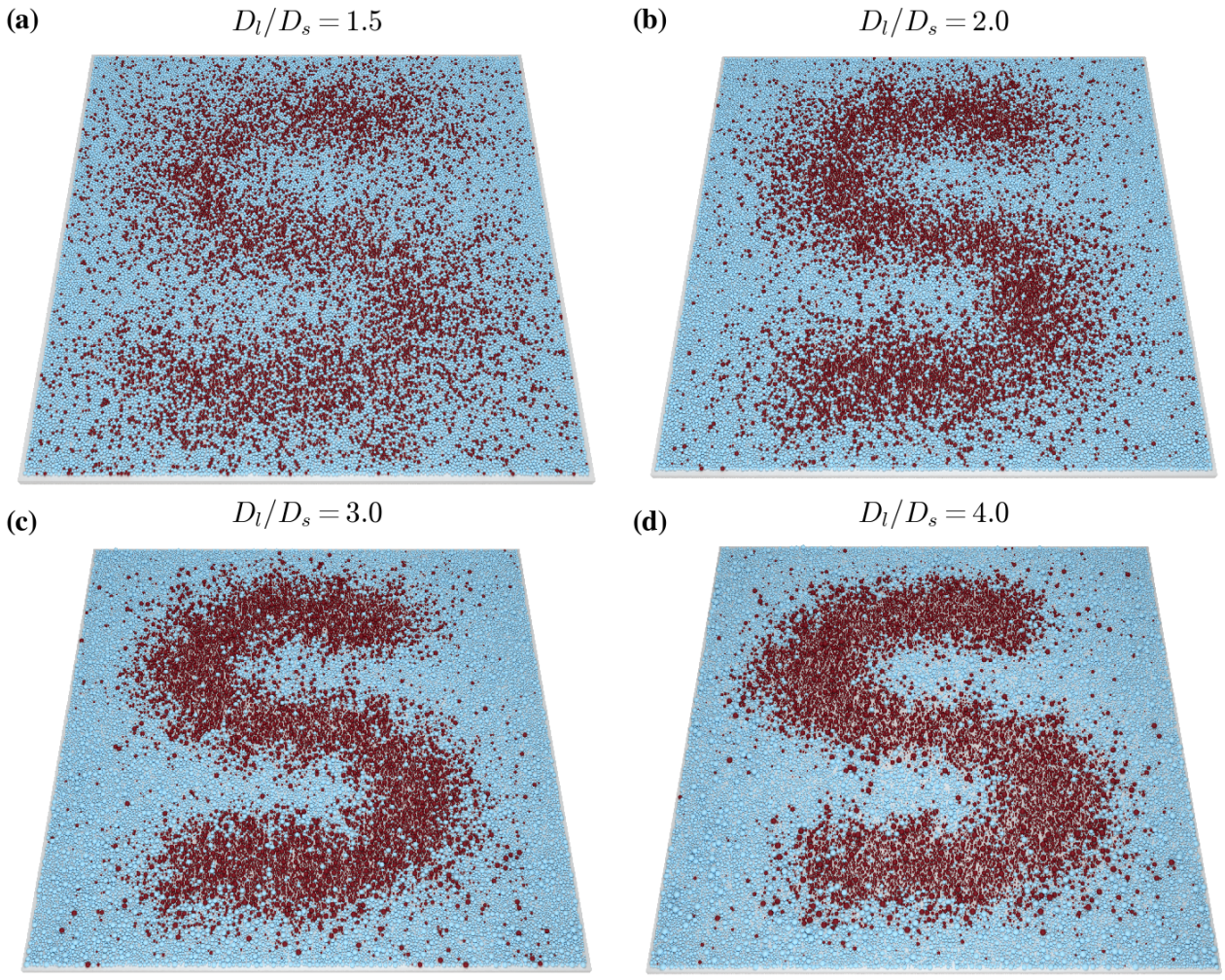

Fig. S5: **Expansion ratio controls pattern fidelity.** Patterns formed by dropping thinker grains with differing large and small diameter ratios. Larger ratios substantially improve pattern fidelity.

zero and no heat fluxes arise in the quiescent fluid. Conversely, in the heat flux tensor all terms except for derivatives of b_i are even moments, and therefore contribute to heat fluxes in the presence of temperature gradients. Fluids with bulk flows ($|\vec{u}| \neq 0$) will have contributions from first order-corrections to both heat fluxes and the pressure tensor.

S7. PATTERN RESOLUTION IN DROPPED THINKER GRAINS

The ability of thinkers to form and maintain patterns was principally a function of the ratio of their large and small diameter states. Figure S5 shows this trend for diameter ratios ranging from $D_l/D_s = 1.5 \rightarrow 4$.

S8. DESCRIPTION OF SUPPLEMENTAL VIDEOS

S8.1. Supplemental video S1

In this video, two species of thinker particles are dropped into a hard-sided box. They fall under a vertical force, while a drag force (linear in velocity) causes them to slowly lose energy and settle into a layer. Feedback control of thinker diameter allows the two species to separate and form a pre-programmed pattern.

S8.2. Supplemental video S2

In this video, two species of thinker particles are continuously agitated while contained in a hard-sided box. Feedback control of thinker diameters allow the two species to form patterns, which are changed over time. The thinkers can therefore write sequences of symbols, as shown here with an equation.

---

[1] L. Zhu, E. Lauga, and L. Brandt, Physics of fluids **24**, 051902 (2012).
[2] P. Romanczuk, M. Bär, W. Ebeling, B. Lindner, and L. Schimansky-Geier, The European Physical Journal Special Topics **202**, 1 (2012).
[3] A. Doostmohammadi, J. Ignés-Mullol, J. M. Yeomans, and F. Sagués, Nature communications **9**, 1 (2018).
[4] T. Sanchez, D. T. N. Chen, S. J. DeCamp, M. Heymann, and Z. Dogic, Nature **491**, 431 (2012), ISSN 1476-4687, URL `http://www.nature.com/articles/nature11591`.
[5] I. Buttinoni, J. Bialké, F. Kümmel, H. Löwen, C. Bechinger, and T. Speck, Physical Review Letters **110**, 238301 (2013), publisher: American Physical Society, URL `https://link.aps.org/doi/10.1103/PhysRevLett.110.238301`.
[6] J. Palacci, S. Sacanna, A. P. Steinberg, D. J. Pine, and P. M. Chaikin, Science **339**, 936 (2013), publisher: American Association for the Advancement of Science, URL `http://www.science.org/doi/full/10.1126/science.1230020`.
[7] C. Bechinger, R. Di Leonardo, H. Löwen, C. Reichhardt, G. Volpe, and G. Volpe, Reviews of Modern Physics **88**, 045006 (2016).
[8] J. Tailleur and M. Cates, Physical review letters **100**, 218103 (2008).
[9] A. Bricard, J.-B. Caussin, N. Desreumaux, O. Dauchot, and D. Bartolo, Nature **503**, 95 (2013).
[10] A. Bricard, J.-B. Caussin, D. Das, C. Savoie, V. Chikkadi, K. Shitara, O. Chepizhko, F. Peruani, D. Saintillan, and D. Bartolo, Nature communications **6**, 1 (2015).
[11] J. Deseigne, O. Dauchot, and H. Chaté, Physical review letters **105**, 098001 (2010).
[12] M. C. Marchetti, J.-F. Joanny, S. Ramaswamy, T. B. Liverpool, J. Prost, M. Rao, and R. A. Simha, Reviews of modern physics **85**, 1143 (2013).
[13] T. H. Tan, A. Mietke, J. Li, Y. Chen, H. Higinbotham, P. J. Foster, S. Gokhale, J. Dunkel, and N. Fakhri, Nature **607**, 287 (2022).
[14] H. Leff and A. F. Rex, *Maxwell's Demon 2 Entropy, Classical and Quantum Information, Computing* (CRC Press, 2002).
[15] J. Toner and Y. Tu, Phys. Rev. E **58**, 4828 (1998).
[16] J. Gelles and R. Landick, Cell **93**, 13 (1998).
[17] J. F. Sydow and P. Cramer, Current opinion in structural biology **19**, 732 (2009).
[18] A. L. Gnatt, P. Cramer, J. Fu, D. A. Bushnell, and R. D. Kornberg, Science **292**, 1876 (2001).
[19] I. Artsimovitch and R. Landick, Proceedings of the National Academy of Sciences **97**, 7090 (2000).
[20] V. R. Tadigotla, D. Ó. Maoiléidigh, A. M. Sengupta, V. Epshtein, R. H. Ebright, E. Nudler, and A. E. Ruckenstein, Proceedings of the National Academy of Sciences **103**, 4439 (2006).
[21] H. Kettenberger, K.-J. Armache, and P. Cramer, Cell **114**, 347 (2003).
[22] D. A. Erie, O. Hajiseyedjavadi, M. C. Young, and P. H. von Hippel, Science **262**, 867 (1993).
[23] M. T. Marr and J. W. Roberts, Molecular cell **6**, 1275 (2000).
[24] E. A. Abbondanzieri, W. J. Greenleaf, J. W. Shaevitz, R. Landick, and S. M. Block, Nature **438**, 460 (2005).
[25] J. M. Parrondo, J. M. Horowitz, and T. Sagawa, Nature physics **11**, 131 (2015).
[26] F. J. Cao and M. Feito, Physical Review E **79**, 041118 (2009).
[27] T. M. Cover and J. A. Thomas, *Elements of information theory* (Wiley-Interscience, 2006).
[28] P. J. Flory and J. Rehner, The Journal of Chemical Physics **11**, 512 (1943), URL `https://doi.org/10.1063/1.1723791`.
[29] L. G. Treloar, *The physics of rubber elasticity* (OUP Oxford, 1975).
[30] K. Wojciechowski and A. Brańka, Physics Letters A **134**, 314 (1989), ISSN 0375-9601, URL `https://www.sciencedirect.com/science/article/pii/0375960189906427`.
[31] B. VanSaders, J. Dshemuchadse, and S. C. Glotzer, Physical Review Materials **2**, 063604 (2018).
[32] C. Cercignani, R. Illner, and M. Pulvirenti, *The Mathematical Theory of Dilute Gases*, Applied Mathematical Sciences (Springer New York, 1994), ISBN 9780387942940.
[33] M. Kardar, *Statistical physics of particles* (Cambridge University Press, 2007).
[34] C. Cercignani, Journal of statistical physics **58**, 817 (1990).
[35] N. E. Korotkov and A. N. Korotkov, *Integrals Related to the Error Function* (CRC Press, 2020).
[36] S. Li, R. Batra, D. Brown, H.-D. Chang, N. Ranganathan, C. Hoberman, D. Rus, and H. Lipson, Nature **567**, 361 (2019).